Geochemical Perspectives Letters

Equilibrium olivine-melt Mg isotopic fractionation explains high δ^{26}Mg values in arc lavas

X.-N. Liu[1*], R.C. Hin[1], C.D. Coath[1], M. van Soest[2], E. Melekhova[3], T. Elliott[1]

OPEN ACCESS

https://doi.org/10.7185/geochemlet.2226

Abstract

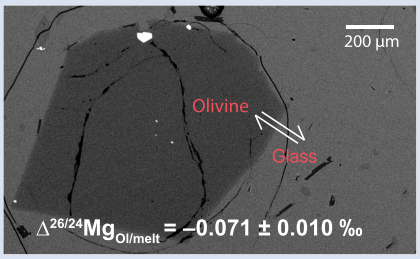

We determined equilibrium Mg isotope fractionation between olivine and melt ($\Delta^{26/24}Mg_{Ol/melt}$) in five, naturally quenched, olivine-glass pairs that were selected to show clear textural and chemical evidence of equilibration. We employed a high-precision, critical mixture double-spiking approach to obtain a weighted mean of $\Delta^{26/24}Mg_{Ol/melt} = -0.071 \pm 0.010$ ‰, for values corrected to a common olivine-glass temperature of 1438 K. As function of temperature, the fractionation can be expressed as $\Delta^{26/24}Mg_{Ol/melt} = (-1.46 \pm 0.26) \times 10^5/T^2$. The samples analysed have variable H_2O content from 0.1 to ~1.2 wt. %, yet no discernible difference in $\Delta^{26/24}Mg_{Ol/melt}$ was evident. We have used this $\Delta^{26/24}Mg_{Ol/melt}$ to revisit the puzzling issue of elevated Mg isotope ratios in arc lavas. In new Mg isotope data on sample suites from the Lesser Antilles and Mariana arcs, we show that primitive samples have MORB-like Mg isotope ratios while the evolved samples tend to have isotopically heavier compositions. The magnitude of this variability is well explained by olivine fractionation during magmatic differentiation as calculated with our new equilibrium $\Delta^{26/24}Mg_{Ol/melt}$.

Received 22 April 2022 | Accepted 1 July 2022 | Published 19 July 2022

Introduction

A burgeoning literature in the mass-dependent variability of major rock forming elements in magmatic samples have the potential to provide novel constraints on source mineralogy and melting processes (*e.g.*, Teng *et al.*, 2017; Soderman *et al.*, 2022), but in many cases the key parameter of isotopic fractionation, *i.e.* the fractionation factor between solid and melt, is insufficiently well constrained to make the most of the observations. In large part, mineral-melt fractionation factors have been determined by the magnitude (or absence) of isotopic variability in sample suites that show well behaved differentiation trends. Although valuable, this strategy convolves the natural complexity of magmatic fractionation with the determination of fractionation factors. A more direct method is to measure the isotope ratios of coexisting equilibrated mineral-melt pairs. This poses the difficulty of obtaining precise measurements on small samples that are demonstrably in equilibrium.

As the third most abundant element in the silicate Earth, there is much interest in the Mg isotopic systematics of magmatic rocks for improving our understanding of igneous processes and broader planetary evolution (*e.g.*, Teng *et al.*, 2010; Hin *et al.*, 2017; Teng, 2017). In interpreting the relatively small isotopic variations in Mg, it is critical to determine a precise fractionation factor between olivine, the major mineral host of Mg, and melt. This parameter is expressed as $\Delta^{26/24}Mg_{Ol/melt}$, defined as $\delta^{26}Mg_{Ol} - \delta^{26}Mg_{melt}$, where δ^{26}Mg is the relative difference in $^{26}Mg/^{24}Mg$ between sample and DSM-3 reference standard. Once determined, $\Delta^{26/24}Mg_{Ol/melt}$ can be used in conjunction with inter-mineral fractionation factors to model Mg isotopic variability in magmatic processes. While inter-mineral fractionations can be determined observationally or by *ab initio* methods, numerical modelling of isotopic exchange between mineral and melt structure is not straight-forward, which has motivated our empirical approach.

There have been two previous attempts to measure $\Delta^{26/24}Mg_{Ol/melt}$. The absence of systematic Mg isotopic variation in a suite of whole rocks with variable MgO contents from Kilauea Iki (Teng *et al.*, 2007) is often cited as evidence for the absence of Mg isotope fractionation during crystallisation. Yet, strictly, this study placed a maximum bound on Mg isotope fractionation during differentiation, namely $|\Delta^{26/24}Mg_{Ol/melt}| \leq 0.07$ ‰. Schiller *et al.* (2017) analysed the Mg isotopic compositions of olivines and rapidly cooled groundmass (dominantly intergrown plagioclase and clinopyroxene) from an angrite meteorite (NWA1670). These authors also reprocessed Mg isotope measurements of olivine and groundmass from Teng *et al.* (2011) to calculate a fractionation factor. Yet, the latter had been originally used to illustrate the effects of diffusive fractionation of Mg isotopes in the chemical potential gradient of zoned minerals. Although Schiller *et al.* (2017) reported those samples closest to elemental Fe-Mg equilibrium, these samples evidently do not constitute an equilibrium assemblage necessary for reliable determination of a fractionation factor. Equally, the bulk olivine phenocrysts in NWA1670 are not in equilibrium with the groundmass, given their Mg/(Mg + Fe) decrease from ~0.9 in their core to ~0.6 in their rim (Jambon *et al.*, 2008).

1. School of Earth Science, University of Bristol, Wills Memorial Building, Bristol BS8 1RJ, UK
2. School of Earth and Space Exploration, ISTB4, Arizona State University, Tempe 85287, AZ, USA
3. Department of Earth Sciences, University of Oxford, South Parks Road, Oxford OX1 3AN, UK
* Corresponding author (email: xl17349@bristol.ac.uk)

Here, we employ the high precision attainable using critical mixture double-spiking (Coath *et al.*, 2017; Hin *et al.*, 2017) to determine $\Delta^{26/24}Mg_{Ol/melt}$ for five carefully selected, equilibrated olivine-glass pairs from ocean island and mid-ocean ridge basalts. Using this value, we then explore the subtly elevated $\delta^{26}Mg$ in arc lavas (Teng *et al.*, 2016) with new analyses of a suite of samples from the Lesser Antilles, as well as a set of archetypical mafic samples from the Mariana arc.

Olivine-melt fractionation factor

We selected samples with petrographic, equilibrium olivine textures in naturally quenched glass from Kilauea (Hawaii), submarine eruptions from Pitcairn and mid-ocean ridge basalts from the Pacific and Indian oceans (for details, see section 1.1 of the Supplementary Information, SI). Prior work on the Hawaii and Pitcairn samples (Jeffcoate *et al.*, 2007) showed an absence of Li isotopic fractionation across the olivine phenocrysts, documenting an absence of late-stage diffusive fractionation. From these potentially suitable samples we then selected individual olivine crystals with a variability in Fo < 1 % across the full cross-sectional electron microprobe profile of the crystal (Fig. 1a). We rejected any olivine which had an olivine-glass Fe-Mg exchange coefficient outside the range of equilibrium values (Ulmer, 1989), namely $K_D^{Ol/melt}$(Fe-Mg) from 0.28 to 0.32 (Fig. 1b).

We analysed micro-drilled spots (cones of 100 µm depth and largest diameter) in these olivines and hand-picked coexisting glass and processed the samples for Mg isotope analysis by critical mixture double-spiking as reported in Hin *et al.* (2017). This method yields a long-term reproducibility of 0.027 ‰ ($\delta^{26}Mg$, 2 s.d.) based on repeated BHVO-2 analyses (see SI section 2.3). We used the pooled $\delta^{26}Mg$ of each phase to yield Mg isotope differences between olivine and melt (*i.e.* glass) for each of the five basalt samples (Table S-1). Olivine thermometry (Putirka, 2005) indicates that equilibration temperatures of the five samples varied between 1379 and 1481 K (see SI section 1.2). Using a $1/T^2$ scaling, we corrected the isotope differences to a single, average temperature of 1438 K, yielding $\Delta^{26/24}Mg_{Ol/melt}$ between −0.045 ± 0.036 ‰ and −0.086 ± 0.016 ‰ (Fig. 1b, Table S-2). These values are consistent with each other and yield a weighted mean of $\Delta^{26/24}Mg_{Ol/melt} = -0.071 \pm 0.010$ ‰ or $\Delta^{26/24}Mg_{Ol/melt} = (-1.46 \pm 0.26) \times 10^5/T^2$ (T in Kelvin). For the first time, we thus show that olivine in equilibrium with melt is significantly enriched in light Mg isotopes and we recommend that our olivine-melt fractionation factor should

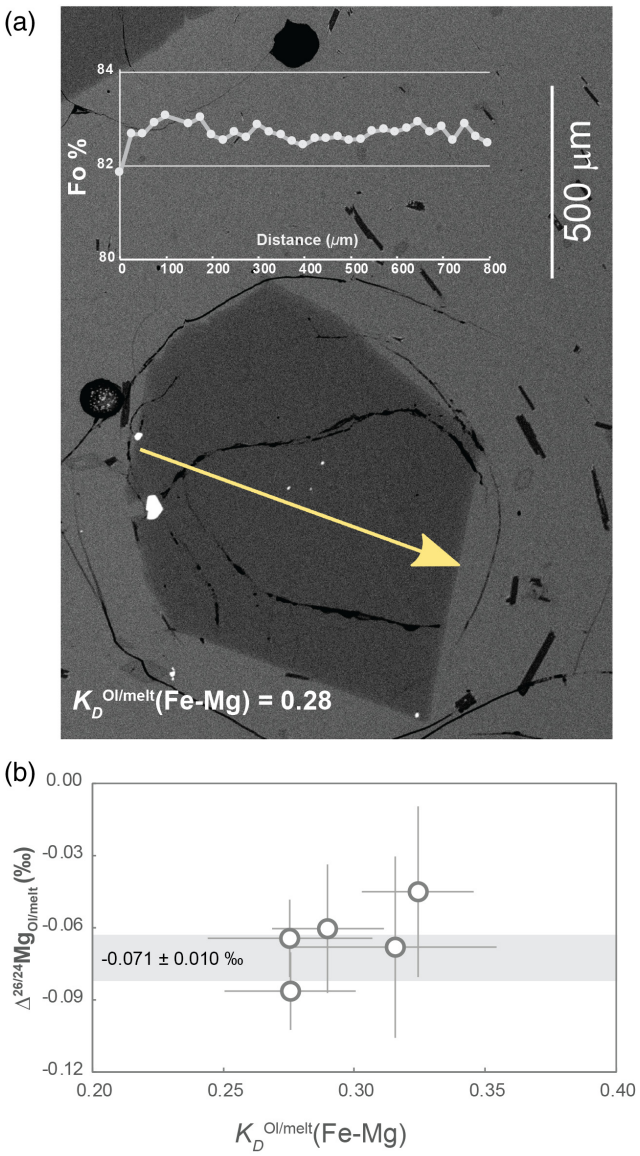

Figure 1 **(a)** Backscattered electron microscope image of an olivine-glass pair (PN3-10), together with electron microprobe traverse of olivine Fo content. **(b)** Measured $\Delta^{26/24}Mg_{Ol/melt}$, corrected to a common temperature (1438 K), plotted against Fe-Mg distribution coefficients.

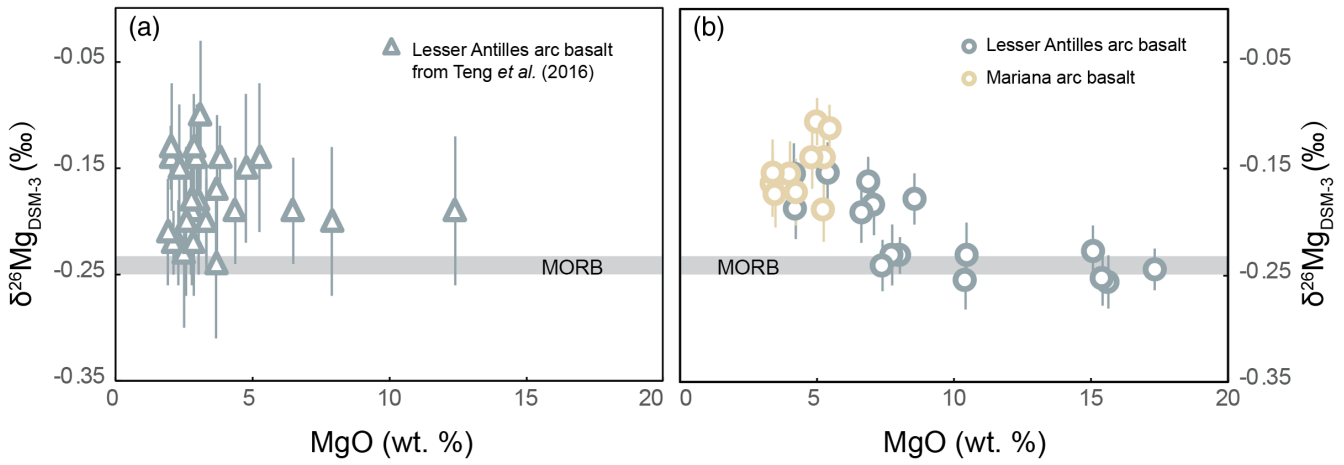

Figure 2 $\delta^{26}Mg$ against MgO for **(a)** Lesser Antilles lavas from Teng *et al.* (2016) and **(b)** Lesser Antilles and Mariana lavas from this study. MORB reference value is −0.24 ± 0.01 ‰ (2 s.e.); see Supplementary Information section 3.4.

be considered when modelling Mg isotope fractionation in magmatic process. We also tried to experimentally determine $\Delta^{26/24}Mg_{Ol/melt}$ but this attempt unfortunately failed, most likely due to thermal diffusion (see SI section 1.3).

The Hawaiian and Pitcairn samples have water contents of ~0.1–0.4 wt. % (*e.g.*, Hauri, 2002) and ~1.2 wt. % (Aubaud *et al.*, 2006), respectively. MORB samples generally have low water contents around 0.1 to 0.2 wt. % (*e.g.*, Sobolev *et al.*, 1996). Water decreases the Mg-O coordination number of silicate melt (Mookherjee *et al.*, 2008), which may lead to a preference for heavier isotopes. Nonetheless, the $\Delta^{26/24}Mg_{Ol/melt}$ determined from Hawaiian, Pitcairn and the three MORB olivine-glass pairs are all within the analytical error (Fig. 1b). The absence of a discernible effect on the fractionation factor for water contents up to 1.2 wt. % leads us to assume that water has a limited effect on $\Delta^{26/24}Mg_{Ol/melt}$.

Elevated δ^{26}Mg in arc lavas

Teng *et al.* (2016) analysed arc lavas from Martinique, Lesser Antilles, and reported δ^{26}Mg slightly higher than MORB

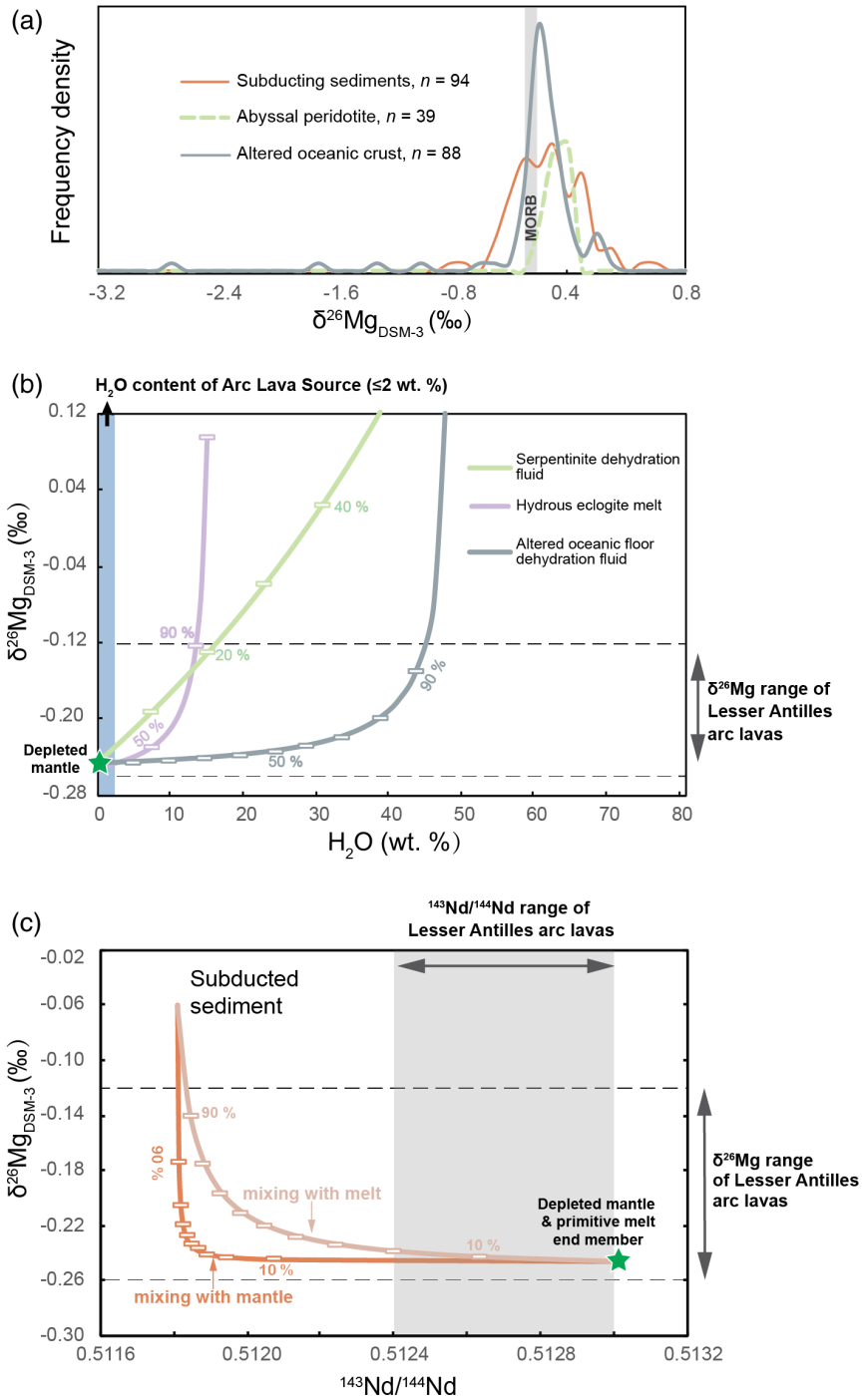

Figure 3 **(a)** Frequency density plot of δ^{26}Mg of subducted materials. **(b)** Modelled δ^{26}Mg against H_2O from mixing depleted mantle with dehydration fluids and hydrous melt. **(c)** Modelled δ^{26}Mg against $^{143}Nd/^{144}Nd$ from mixing depleted mantle with subducted sediments (See SI section 3.5 for more details).

(Fig. 2a), which they attributed to subduction zone processes. As discussed by Teng *et al.* (2016), however, it is not clear that subduction zone components have the leverage to sufficiently perturb the δ^{26}Mg of the mantle wedge, given mixing constraints from other elemental and isotopic tracers. To further explore this intriguing phenomenon, we have made high precision, critical mixture double-spiked analyses of Lesser Antilles samples from a wider range of islands, including rare primitive lavas from the southern arc. We also analysed a well characterised set of samples from the Mariana arc (see SI sections 3.2, 3.3). Our new measurements show the Lesser Antilles lavas have MORB-like δ^{26}Mg in the most MgO-rich samples, while more evolved lavas have δ^{26}Mg up to 0.12 ‰ higher (Figs. 2b, S-5). All the Mariana arc lavas plot together with the less mafic Lesser Antilles samples (Fig. 2b, Table S-5). To better understand the causes of the higher δ^{26}Mg in some arc lavas, we initially concentrate on the Lesser Antilles example, for which we have samples with a wider compositional range.

First, we reconsider the possible role of subduction components (Fig. 3a). The results of binary mixing calculations (see SI section 3.5 for details) between the sub-arc mantle and potential subduction inputs are illustrated in Figure 3b, c. Fluids released from subducted oceanic crust and serpentinite are naturally water-rich, over 50 wt. % and 80 wt. % H_2O respectively, while the MgO concentrations of these fluids are generally low, less than 1 wt. % in oceanic crust dehydration fluid and about 6 wt. % in serpentinite dehydration fluid (Manning, 2004; Kessel *et al.*, 2005; Scambelluri *et al.*, 2015). Hydrous melts generated from eclogite are again enriched in water (over 15 wt. %) but also low in Mg (less than 2.5 wt. %) (Gervasoni *et al.*, 2017). The amount of these slab-derived fluid phases added to the mantle wedge is constrained by a maximum 2 wt. % H_2O in the mantle source (assuming at most 10 wt. % H_2O in primitive arc magmas and 20 % partial melting degree). As a result, the Mg isotopic perturbation of the arc lava source is inappreciably influenced by plausible contributions of slab-derived fluids (Fig. 3b). The subducting sediments are isotopically heavier than MORB (Fig. 3a), but a contribution over 90 wt. % sediment would be required in the source of the Lesser Antilles lavas to reproduce the highest δ^{26}Mg. Such an amount of sediment is equally inconsistent with the ^{143}Nd/^{144}Nd of the arc lavas (Fig. 3c).

Our high precision analyses allow some structure to be discerned in the variability of δ^{26}Mg in the Lesser Antilles samples, which can have been caused by neither weathering nor variable melting depths (see SI section 3.6). The most striking feature is a systematic relationship between δ^{26}Mg and MgO content (Fig. 2b), which implies a role for magmatic differentiation in fractionating Mg isotopes. When dealing with the effects of differentiation in bulk samples, however, it is important to evaluate crystal accumulation. This is especially marked for Mg given the high MgO contents of olivine. Therefore, we analysed the compositions of olivine crystals in our Lesser Antilles samples. Three samples (WIC19, LSS1 & LAS1) have unexpectedly Fo-rich, xenocrystic olivines compared with their bulk Mg# (Fig. 4a, SI section 3.7). Moreover, disequilibrium textures between olivine crystals and groundmass are observed in the thin sections of these samples (Fig. 4b).

We have divided Lesser Antilles arc samples into four groups (Fig. 4a, c, d). Five samples with high MgO are dubbed "primitive", as detailed petrological experiments have identified such compositions are plausibly in equilibrium with the mantle wedge (see SI section 3.2). They have δ^{26}Mg values within error of MORB (Fig. 4c). Seven samples are grouped as "evolved" and display elevated δ^{26}Mg values. The three samples that contain Fo-rich olivine xenocrysts are named "xeno" and these also have MORB-like δ^{26}Mg values. A single troctolite sample, LAE3, is labelled "cumulate". The Mariana samples are all geochemically

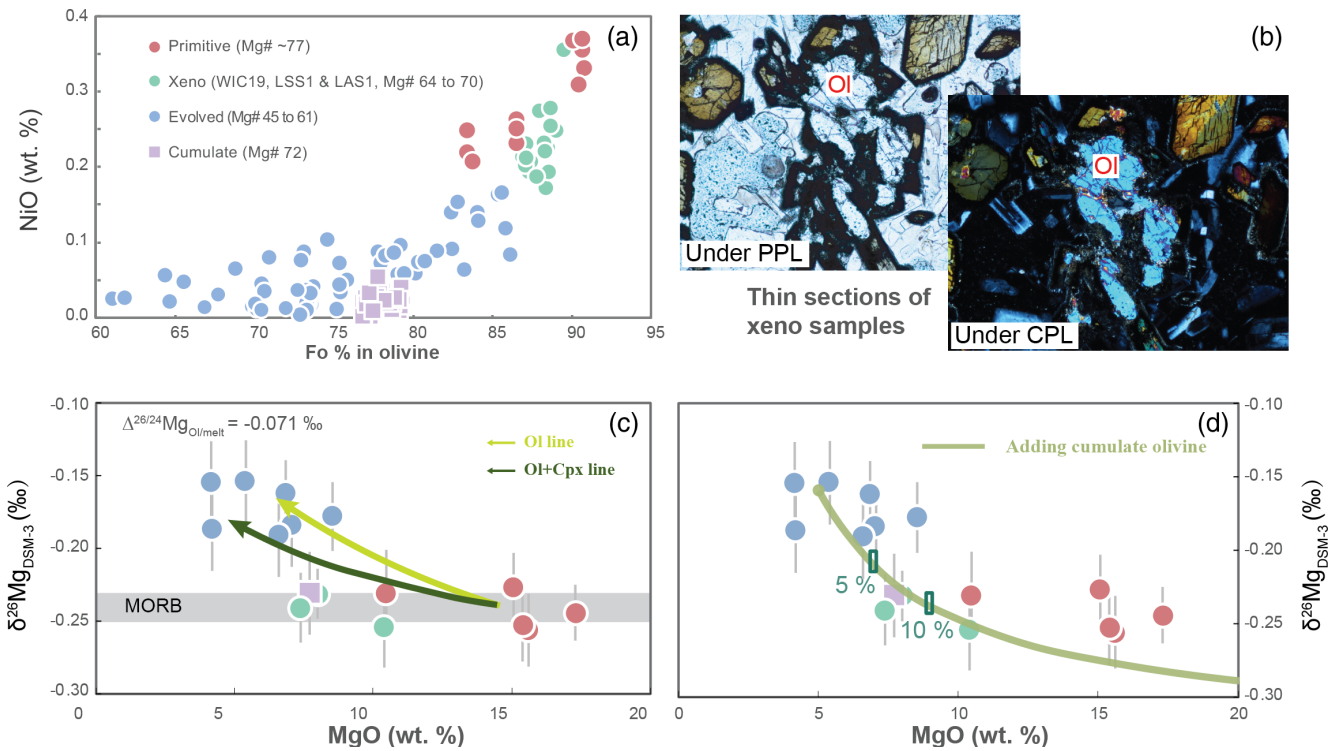

Figure 4 **(a)** Electron microprobe analyses of Lesser Antilles olivines plotted in groups according to bulk Mg# of host magmas. **(b)** Thin-section images of disequilibrium olivines in "xeno" group samples. **(c)** Modelled δ^{26}Mg evolution during two main differentiation paths. **(d)** Modelled effect on δ^{26}Mg of cumulate olivine addition to an "evolved" sample composition.

similar to the "evolved" group and also have elevated δ^{26}Mg values.

Unlike in the Marianas, the magma differentiation paths of Lesser Antilles arc lavas are well constrained (see SI section 3.8). Two liquid lines of descent have been identified: one involves co-crystallisation of olivine and clinopyroxene at high pressure, while at low pressures, olivine is the only liquidus phase (*e.g.*, Stamper *et al.*, 2014). We model the variations in δ^{26}Mg that result from these two differentiation trends using our new $\Delta^{26/24}Mg_{Ol/melt}$ and $\Delta^{26/24}Mg_{Cpx/melt}$ (derived by combining $\Delta^{26/24}Mg_{Ol/melt}$ with literature $\Delta^{26/24}Mg_{Cpx/Ol}$, SI section 3.9). Both 20 % olivine fractionation (Ol line) and the co-crystallisation of 20 % olivine and 20 % clinopyroxene (Ol + Cpx line) reproduce the elevated δ^{26}Mg of many evolved lavas (Fig. 4c), as a result of olivine crystallisation. The lower δ^{26}Mg data of the "xeno" samples are well reproduced by olivine accumulation (Fig. 4d) in more evolved samples. The composition of the troctolite cumulate (LAE3) is consistent with its crystallisation from a melt with elevated δ^{26}Mg ≈ −0.16 ‰ given our $\Delta^{26/24}Mg_{Ol/melt}$. We infer that the relatively low MgO and high δ^{26}Mg of the Mariana samples (Fig. 2b) reflect a differentiation process similar to that experienced by the Lesser Antilles "evolved" samples.

In conclusion, we have replicated elevated δ^{26}Mg in Lesser Antilles arc lavas and further shown this to be a common characteristic in Mariana arc lavas. However, our more precise analyses reveal that the elevated δ^{26}Mg is only evident in more evolved, basaltic andesite compositions. Using the equilibrium $\Delta^{26/24}Mg_{Ol/melt}$ we determined, we can model the increase in δ^{26}Mg from MORB-like values in primitive arc lavas as a natural consequence of magmatic differentiation. This illustrates the importance of a well determined solid-melt fractionation factor in interpreting subtle differences in stable isotope ratios.

Acknowledgements

Carolyn Taylor and Stuart Kearns are thanked for their help in the lab. We also thank Richard Robertson and Bernard Bourdon for providing Lesser Antilles and Pitcairn samples respectively. This work was funded by NERC grant NE/L007428/1 and ERC Grant 885531 NONUNE. X.-N. Liu was supported by a CSC scholarship.

Editor: Ambre Luguet

Additional Information

Supplementary Information accompanies this letter at https://www.geochemicalperspectivesletters.org/article2226.

Cite this letter as: Liu, X.-N., Hin, R.C., Coath, C.D., van Soest, M., Melekhova, E., Elliott, T. (2022) Equilibrium olivine-melt Mg isotopic fractionation explains high δ^{26}Mg values in arc lavas. *Geochem. Persp. Let.* 22, 42–47. https://doi.org/10.7185/geochemlet.2226

References

Aubaud, C., Pineau, F., Hekinian, R., Javoy, M. (2006) Carbon and hydrogen isotope constraints on degassing of CO_2 and H_2O in submarine lavas from the Pitcairn hotspot (South Pacific). *Geophysics Research Letters* 33, L02308. https://doi.org/10.1029/2005GL024907

Coath, C.D., Elliott, T., Hin, R.C. (2017) Double-spike inversion for three-isotope systems. *Chemical Geology* 451, 78–89. https://doi.org/10.1016/j.chemgeo.2016.12.025

Gervasoni, F., Klemme, S., Rohrbach, A., Griltzner, T., Berndt, J. (2017) Experimental constraints on mantle metasomatism caused by silicate and carbonate melts. *Lithos* 282–283, 173–186. https://doi.org/10.1016/j.lithos.2017.03.004

Hauri, E. (2002) SIMS analysis of volatiles in silicate glasses, 2: isotopes and abundances in Hawaiian melt inclusions. *Chemical Geology* 183, 115–141. https://doi.org/10.1016/S0009-2541(01)00374-6

Hin, R.C., Coath, C.D., Carter, P.J., Nimmo, F., Lai, Y.-J., Pogge von Strandmann, P.A.E., Willbold, M., Leinhardt, Z.M., Walter, M.J., Elliott, T. (2017) Magnesium isotope evidence that accretional vapour loss shapes planetary compositions. *Nature* 549, 511–515. https://doi.org/10.1038/nature23899

Jambon, A., Boudouma, O., Fonteilles, M., Le Guillou, C., Badia, D., Barrat, J.A. (2008) Petrology and mineralogy of the angrite Northwest Africa 1670. *Meteoritics & Planetary Science* 43, 1783–1795. https://doi.org/10.1111/j.1945-5100.2008.tb00643.x

Jeffcoate, A.B., Elliott, T., Kasemann, S.A., Ionov, D., Cooper, K., Brooker, R. (2007) Li isotope fractionation in peridotites and mafic melts. *Geochimica et Cosmochimica Acta* 71, 202–218. https://doi.org/10.1016/j.gca.2006.06.1611

Kessel, R., Schmidt, M.W., Ulmer, P., Pettke, T. (2005) Trace element signature of subduction-zone fluids, melts and supercritical liquids at 120–180 km depth. *Nature* 437, 724–727. https://doi.org/10.1038/nature03971

Manning, C.E. (2004) The chemistry of subduction-zone fluids. *Earth and Planetary Science Letters* 223, 1–16. https://doi.org/10.1016/j.epsl.2004.04.030

Mookherjee, M., Stixrude, L., Karki, B. (2008) Hydrous silicate melt at high pressure. *Nature* 452, 983–986. https://doi.org/10.1038/nature06918

Putirka, K.D. (2005) Mantle potential temperatures at Hawaii, Iceland, and the mid-ocean ridge system, as inferred from olivine phenocrysts: Evidence for thermally driven mantle plumes. *Geochemistry, Geophysics, Geosystems* 6, Q05L08. https://doi.org/10.1029/2005GC000915

Scambelluri, M., Pettke, T., Cannao, E. (2015) Fluid-related inclusions in Alpine high-pressure peridotite reveal trace element recycling during subduction-zone dehydration of serpentinized mantle (Cima di Gagnone, Swiss Alps). *Earth and Planetary Science Letters* 429, 45–59. https://doi.org/10.1016/j.epsl.2015.07.060

Schiller, M., Dallas, J.A., Creech, J., Bizzarro, M., Baker, J.A. (2017) Tracking the formation of magma oceans in the Solar System using stable magnesium isotopes. *Geochemical Perspectives Letters* 3, 22–31. https://doi.org/10.7185/geochemlet.1703

Sobolev, A.V., Chaussidon, M. (1996) H_2O concentrations in primary melts from supra-subduction zones and mid-ocean ridges: Implications for H_2O storage and recycling in the mantle. *Earth and Planetary Science Letters* 137, 45–55. https://doi.org/10.1016/0012-821X(95)00203-O

Soderman, C.R., Shorttle, O., Matthews, S., Williams, H.M. (2022) Global trends in novel stable isotopes in basalts: Theory and observations. *Geochimica et Cosmochimica Acta* 318, 388–414. https://doi.org/10.1016/j.gca.2021.12.008

Stamper, C.C., Melekhova, E., Blundy, J.D., Arculus, R.J., Humphreys, M.C.S., Brooker, R.A. (2014) Oxidised phase relations of a primitive basalt from Grenada, Lesser Antilles. *Contributions to Mineralogy and Petrology* 167, 954. https://doi.org/10.1007/s00410-013-0954-6

Teng, F.-Z. (2017) Magnesium Isotope Geochemistry. *Reviews in Mineralogy and Geochemistry* 82, 219–287. https://doi.org/10.2138/rmg.2017.82.7

Teng, F.-Z., Wadhwa, M., Helz, R.T. (2007) Investigation of magnesium isotope fractionation during basalt differentiation: Implications for a chondritic composition of the terrestrial mantle. *Earth and Planetary Science Letters* 261, 84–92. https://doi.org/10.1016/j.epsl.2007.06.004

Teng, F.-Z., Li, W.-Y., Ke, S., Marty, B., Dauphas, N., Huang, S., Wu, F.-Y., Pourmand, A. (2010) Magnesium isotopic composition of the Earth and chondrites. *Geochimica et Cosmochimica Acta* 74, 4150–4166. https://doi.org/10.1016/j.gca.2010.04.019

Teng, F.-Z., Dauphas, N., Helz, R.T., Gao, S., Huang, S. (2011) Diffusion-driven magnesium and iron isotope fractionation in Hawaiian olivine. *Earth and Planetary Science Letters* 308, 317–324. https://doi.org/10.1016/j.epsl.2011.06.003

Teng, F.-Z., Hu, Y., Chauvel, C. (2016) Magnesium isotope geochemistry in arc volcanism. *Proceedings of the National Academy of Sciences* 113, 7082–7087. https://doi.org/10.1073/pnas.1518456113

Teng, F.-Z., Watkins, J.M., Dauphas, N. (2017) Non-Traditional Stable Isotopes. *Reviews in Mineralogy and Geochemistry* 82. The Mineralogical Society of America. https://doi.org/10.1515/9783110545630

Ulmer, P. (1989) The dependence of the Fe^{2+}-Mg cation-partitioning between olivine and basaltic liquid on pressure, temperature and composition. *Contributions to Mineralogy and Petrology* 101, 261–273. https://doi.org/10.1007/BF00375311

Geochemical Perspectives Letters

Equilibrium olivine-melt Mg isotopic fractionation explains high δ^{26}Mg values in arc lavas

X.-N. Liu(刘效宁), R.C. Hin, C.D. Coath, M. van Soest, E. Melekhova, T. Elliott

Supplementary Information

The Supplementary Information includes:

1. Olivine-Glass Pair Samples

1.1 Sample selection and drilling

Five olivine-glass pairs from naturally quenched oceanic basalt were chosen to constrain the olivine-melt Mg isotopic fractionation factor. Two of them are from OIB samples (PN3-10 and AH-1) and three are from MORB samples (5/15g, D27-3 and 37DS-1). PN3-10 is picritic basalt from the Pitcairn hotspot (Hekinian *et al*., 2003; Bourdon and Van Orman, 2009 and references therein) and AH-1 is a basalt from a historic Pu'u O'o flow, Kilauea, Hawaii (Jeffcoate *et al*., 2007). 5/15g is from the southwestern Indian Ridge (Robinson, 1998). D27-3 is from the mid-Atlantic ridge (Niu and Batiza, 1994; Graham *et al.*, 1996; Regelous *et al.*, 2009) and 37DS-1 is from the South Kolbeinsey ridge in the Atlantic Ocean (Devey *et al*., 1994).

Li isotopes are a sensitive indicator of potential, late-stage diffusive perturbation of phenocryst compositions (*e.g*., Parkinson *et al*., 2007; Gallagher and Elliott, 2009) which may also affect Mg isotope ratios (Teng *et al*., 2011; Oeser *et al*., 2015). The absence of zoning in Li isotopes in olivine in the two OIB samples (Jeffcoate *et al*., 2007, and unpublished data) was therefore a major motivation to select these two samples.

For MORB samples pristine olivine grains were also analysed by electron microprobe for their chemical compositions. We selected the olivines with Fo variation less 1 % and Fe-Mg distribution coefficient in equilibrium with the host glass (*i.e*. $K_D^{Ol/melt}$(Fe-Mg) in the range 0.28–0.32; Ulmer, 1989) (see Table S-6).

Fragments of OIB samples were mounted in epoxy prior to sanding and polishing to expose olivine and glass (see Fig. S-1 for an example of PN3-10 fragments). Olivines in MORB samples were hand-picked under an optical binocular microscope and then set in epoxy resin and polished. Olivines in OIB and MORB samples were drilled using a New Wave Research micro-mill. We obtained separate aliquots from four olivines for PN3-10, three olivines for AH-

1, two olivines for 5/15g and 37DS-1, and a single grain of olivine was drilled for sample D27-3. Conical tungsten-carbide drill bits were pre-cleaned by sonication in acetone followed by sonication in high-purity water. For each olivine sample, four or five spots of 100 μm depth and 100 μm (top of cone) width were drilled with a ~5 μL droplet of Milli-Q water (purified water with a resistivity of 18.2 MΩ cm) covering the surface to collect the drilled olivine powder. The water-olivine slurry was transferred with a 20 μL pipette tip into pre-cleaned PFA beakers after each drilled spot. Subsequently, HF-HNO_3 mixtures were added for digestion.

Glass samples from PN3-10 were also obtained by micro-drilling (15 drill spots, see Fig. S-1). Glass from MORB and AH-1 were obtained by hand-picking glass chips under a binocular microscope with the criterion of totally transparent glass, with clean surfaces and obvious glassy lustre. The picked chips were then cleaned in an ultrasonic bath with acetone and Milli-Q water three times separately.

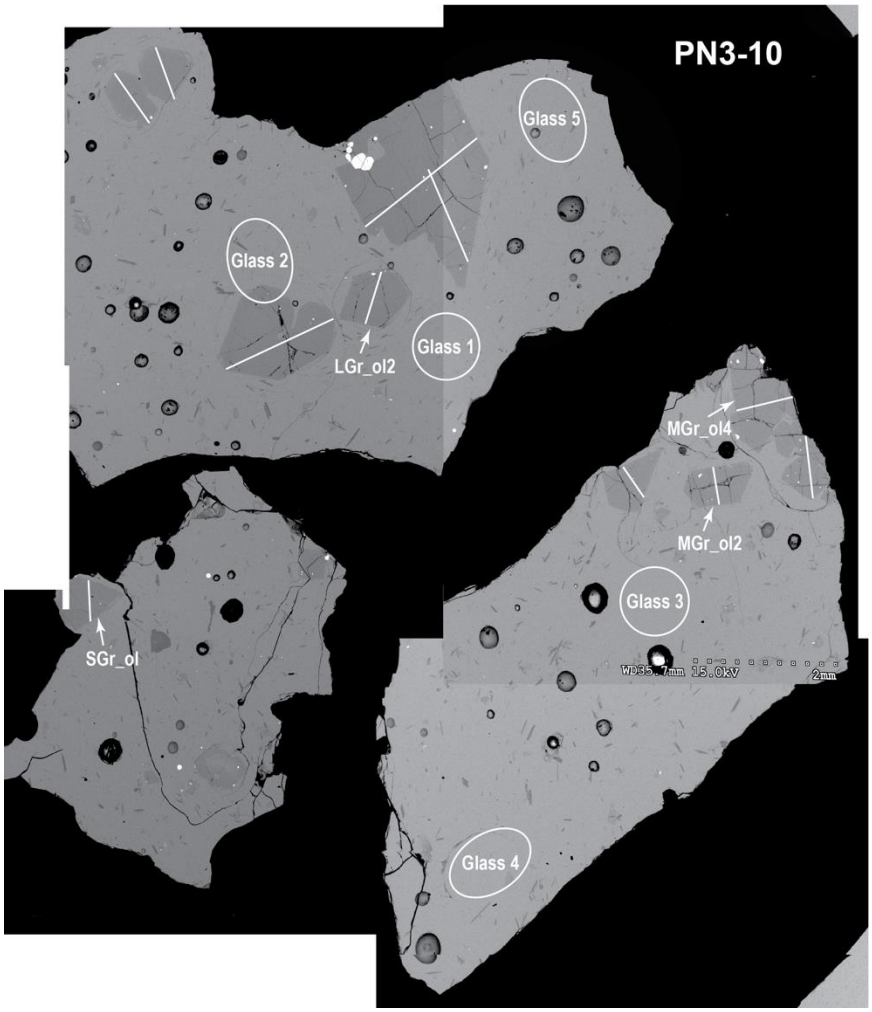

Figure S-1 Locations of microprobe profiles in olivine and drill spots in olivine and glass in PN3-10. Glass 2 was rejected as the drill did not align well and therefore this sample contains some olivine. Unlabelled microprobe profiles are on olivine that did not meet our selection criteria for chemical equilibrium (see main text and SI Section 1.1).

1.2 Temperature estimates for olivine-glass pairs

Since the olivine-glass pairs are all in equilibrium, we use the olivine thermometer of Putirka (2005) and Putirka *et al*. (2007), which is mainly based on the partitioning of Mg and Fe between olivine and glass, to estimate the olivine saturation temperature (Roeder and Emslie, 1970). We used their equations for Mg and Fe both with and without

composition dependence (Putirka, 2005; Putirka *et al.*, 2007). We found that the calculated results from the different equations are consistent with each other (less than 50 °C difference). Considering the analytical uncertainties of Fe and Mg contents in olivine (usually 1 % relative error) and the resulting temperature uncertainties, this 50 °C difference is negligible, and we thus use the average value of calculated temperatures (Table S-2).

1.3 Attempt of determining olivine melt fractionation factor through experiment

As well as using natural samples (Section 1.1), we also tried to constrain the olivine-melt Mg isotopic fractionation factor through previously published experiments that investigated differentiation of a high-MgO primitive basalt from St Vincent, Lesser Antilles (Melekhova *et al.*, 2013, 2015). We selected experiment RSV49_2 (Fig. S-2) with initial water content of 0.6 wt. %. The glass water content in this experimental run product is similar to natural samples analysed in this study. The experiment material was contained in an Au-Pd double capsule (Fig. S-3), aimed to minimise chemical potential gradients in H_2O, and was carried out at 1350 °C and 1.0 GPa (Melekhova *et al*., 2015). It is believed to have attained chemical equilibrium (Fe-Mg exchange coefficient). It has only glass in the inner capsule and unzoned olivine and melt in outer capsule (see details in Melekhova *et al*., 2015). Olivine grains, found at one edge of the presumably cooler outer capsule, are unzoned and around 100 μm in diameter (Fig. S-2). Samples of these olivine grains and glass from different parts of the charge (Fig. S-3) were obtained by micro-drilling using New Wave Research micro-mill, about five 50 to 100 μm drilling spots for olivine and about five 200 μm drilling spot for glass sample (Fig. S-3), in the same manner as described in Section 1.1.

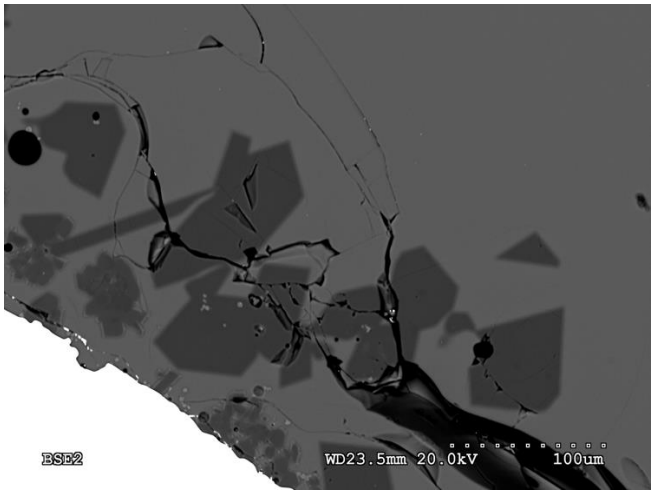

Figure S-2 BSE image of RSV49_2 with olivine (dark grey) and glass (grey).

There are significant Mg isotope differences in glass across the experimental sample. We attribute these differences to isotopic fractionation by thermal (Soret) diffusion in the thermal gradient of the experimental charge (Richter *et al*., 2008, 2009). About 0.6 ‰ δ^{26}Mg difference was observed in the glass from one side of the outer capsule to another (Fig. S-3). The glass samples with low Mg isotope ratios also have lower Mg/Ca ratio, as also found in the experiments on thermal diffusion performed by Richter *et al*. (2008, 2009). The physical distance from one side to another side is about 7mm. Assuming that the 0.6 ‰ δ^{26}Mg variation is caused by thermal diffusion, a temperature gradient of ~10 °C must have been present during the experiment, based on the experimental thermal diffusion sensitivity Ω of 0.036 ‰/°C/amu obtained by Richter *et al*. (2008). This is a typical temperature gradient for piston-cylinder experiments (*e.g.*, Pickering *et al*., 1998). We also infer from the chemical gradients and the presence of olivine solely in the end of the capsule with highest Mg/Ca and δ^{26}Mg that one end of the charge was the hottest and the other the coldest. Specifically, the significant Mg isotopic fractionation by thermal diffusion makes the experimental material in RSV49 unsuitable to constrain the equilibrium Mg isotope fractionation factor between olivine and melt, but in general this example points to the challenge of laboratory determination of this parameter.

We stress that it has long been recognised that the effects of thermal diffusion evident in the small length scales of typical petrological experiments are rarely replicated for the much less extreme temperature gradients of natural samples (Lesher and Walker,1986). Indeed, Mg isotope fractionation by thermal diffusion has never been identified in natural samples. A study of komatiite Mg isotope compositions (Dauphas *et al*., 2010) argued that there was no evidence for the influence of thermal diffusion, while Xu *et al*. (2020) argued on a theoretical basis that natural thermal gradients cannot lead to Mg isotope fractionation in basaltic melt as it is usually buffered by other kinetic effects. Critically, the randomly sampled drill spots of glass sampled in our OIB sample PN3-10 (Fig. S-1) show all these glass samples have consistent Mg isotope compositions, implying a lack of Mg isotopic fractionation by thermal diffusion (Table S-1).

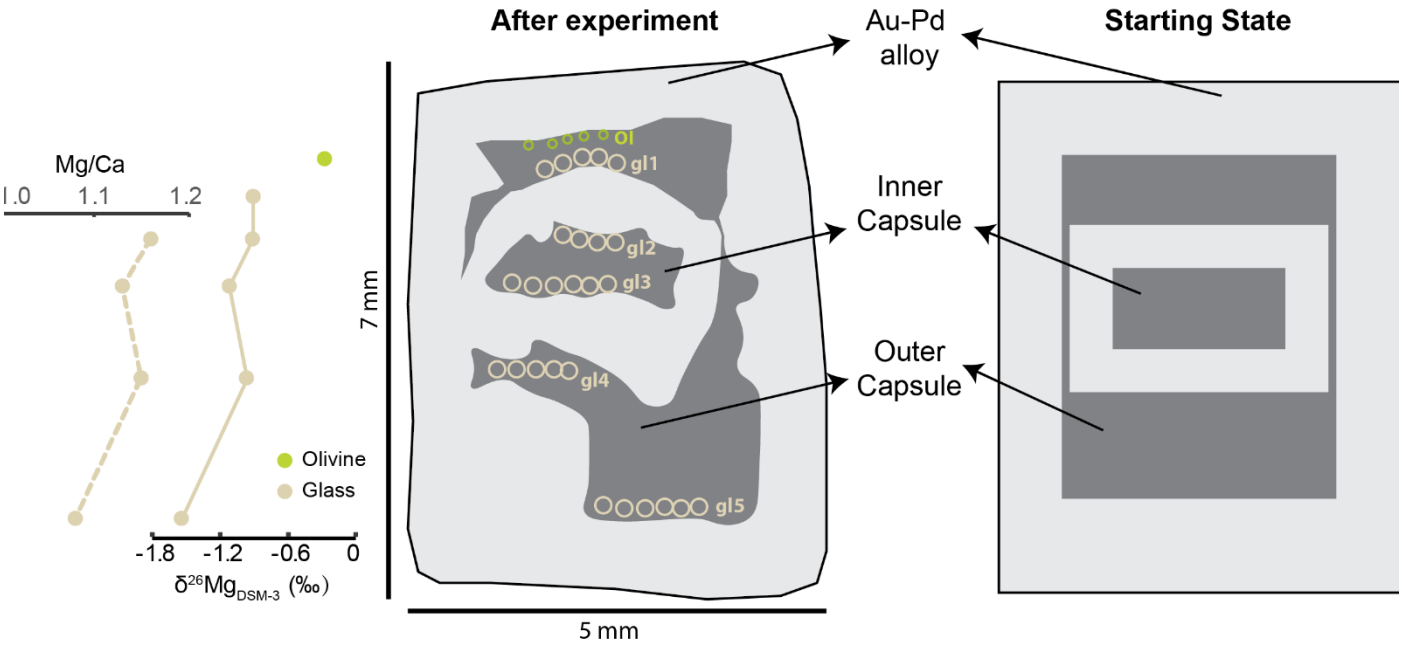

Figure S-3 Mg/Ca and Mg isotopic compositions in various locations of experiment RSV49_2 and a cartoon of its starting state. The symbols in the compositional plots (Mg/Ca and Mg isotope ratio) are aligned in the *y*-axis with their positions in the sketch of the experimental charge of RSV49_2 (after the experiment). Dark grey is the sample material (glass and olivine) and light grey is the Au-Pd capsule. The circles represent the drill spots of olivine and glass samples. Each sample analysed for δ^{26}Mg is a mixture of several drilling spots, *e.g*., gl5 is the mixture of six 200 µm drill spots. Note that this experiment material is made by mixing various, purified oxides, which is why its Mg isotope ratio is outside the range of most natural terrestrial samples. The 2σ error bars for δ^{26}Mg and Mg/Ca ratio data are smaller than the symbols. Mg/Ca ratio was measured from the digested drilled materials on an Element 2 in the Bristol Isotope Group.

Table S-1 Magnesium isotope compositions of picked olivine-glass pairs from natural samples.

Sample ID	$\delta^{26}Mg_{DSM-3}$ (‰)	Pooled 2 s.e.	*N*
AH1_ol3	−0.245	0.020	8
AH1_ol5	−0.233	0.020	8
AH1_ol6	−0.242	0.020	8
AH-1 Olivine, mean	**−0.240**	**0.011**	**24**
AH1_glA	−0.155	0.016	12
AH1_glB	−0.150	0.016	12
AH-1 glass, mean	**−0.152**	**0.011**	**24**
PN3-10 LGr_ol2	−0.342	0.021	7
PN3-10 MGr_ol2	−0.324	0.021	7
PN3-10 MGr_ol4	−0.330	0.021	7
PN3-10 SGr_ol	−0.308	0.021	7
PN3-10 Olivine, mean	**−0.326**	**0.011**	**28**
PN3-10 Glass 1	−0.264	0.028	4
PN3-10 Glass 3	−0.243	0.028	4
PN3-10 Glass 4	−0.285	0.023	6
PN3-10 Glass 5	−0.234	0.021	7
PN3-10 Glass, mean	**−0.256**	**0.012**	**21**
37DS-1 Ol_1	−0.259	0.029	6
37DS-1 Ol_10	−0.264	0.029	6
37DS-1 Olivine, mean	**−0.262**	**0.020**	**12**
37DS-1 glass	**−0.219**	**0.029**	**6**
D27-3 Ol_3	**−0.289**	**0.029**	**6**
D27-3 glass	**−0.224**	**0.024**	**8**
5/15g Ol_4	−0.301	0.013	9
5/15g Ol_5	−0.304	0.013	9
5/15g Olivine, mean	**−0.303**	**0.009**	**18**
5/15g glass	**−0.242**	**0.025**	**10**

Table S-2 Mg isotope fractionation factors between olivine and melt, as calculated based on mean olivine and glass compositions of the samples in Table S-2. $\Delta^{26/24}Mg_{Ol/melt} = \delta^{26}Mg_{Olivine} - \delta^{26}Mg_{glass}$.

	$\Delta^{26/24}Mg_{Ol/melt}$ (‰) (raw)	Temperature (K)	$\Delta^{26/24}Mg_{Ol/melt}$ (‰) (corrected)*	$K_D^{Ol/melt}$ (Fe-Mg)
AH1	−0.088 ± 0.016	1425 ± 80	−0.086 ± 0.016	0.28 ± 0.02
PN3-10	−0.070 ± 0.016	1379 ± 64	−0.064 ± 0.016	0.28 ± 0.03
37DS-1	−0.043 ± 0.036	1481 ± 81	−0.045 ± 0.036	0.32 ± 0.02
27DS-1	−0.065 ± 0.038	1471 ± 104	−0.068 ± 0.038	0.32 ± 0.04
5/15g	−0.061 ± 0.027	1436 ± 34	−0.060 ± 0.027	0.29 ± 0.02
Weighted mean		**1438 ± 81**	**−0.071 ± 0.010**[#]	

*Corrected to the temperature of 1438 K.

[#] The weighted mean (−0.071 ± 0.010 ‰) is calculated from $\sum\frac{\bar{x}}{S^2}/\sum\frac{1}{S^2}$ with variation of two times $\sqrt{1/\sum\frac{1}{S^2}}$.

2. Analytical Methods

2.1 Microprobe measurements

Compositions of olivine and basaltic glass were measured on a CAMECA SX100 electron microprobe at University of Bristol. All data were calibrated to a variety of silicate and oxide standards. Analyses were made using a 20 nA probe current, 1 µm spot size and 10 s counting times (20 s counting times were used for low concentration elements like Ni). Transects over olivine in OIB (PN3-10 and AH-1) and three MORB samples (5/15g, 37DS-1 and D27-3) were set with 10–25 µm spacing between individual spots. The sum of all oxides is 100 ± 2 % (see Tables S-6 and S-7).

2.2 Sample digestion and column chemistry

For the arc lavas, about 50 mg of bulk rock powder of each sample was digested using purified 28 M HF and 15 M HNO_3 (3:1 by volume) in cleaned 30 mL Savillex Teflon beakers on a hotplate at 150 °C. The digestion of glass fragments and drilled olivine materials uses the same procedure but in smaller-size beakers (15 mL or 7 mL). Solutions were dried down and re-dissolved in purified 10 M HCl to digest insoluble fluorides. After complete digestion, all samples were dissolved in 1 M HNO_3 to yield solutions with Mg concentrations of 250 µg mL^{-1} for ion exchange chemistry. Magnesium was separated from matrix elements with two passes through Biorad AG50W-X12 cationic exchange resin. The procedure used here is modified from previous protocols used at the University of Bristol (Pogge von Strandmann *et al*., 2011; Hin *et al*., 2017) in order to maximise removal of some matrix elements (*e.g*., potassium), given the focus of this study on more incompatible element rich lavas as opposed to the previous, meteorite- and peridotite-focussed work. The ion exchange elution scheme is given in Table S-3 and element elution profiles are illustrated in Figs. S-4 and S-5, showing that the Mg concentration peak is well-separated from other matrix elements. Purified 15 M HNO_3 and 30 % hydrogen peroxide (Romil Ltd, SpA grade) were used to attack any potential organics after column chemistry. Yields were monitored based on collected 'splits' before and after the Mg aliquot in each column and were over 99.92 % for all the samples. After the complete chemical separation procedure, the concentration ratios (by mass) between Mg and matrix elements are >700 for K, >800 for Fe, >100 for Mn, >450 for Ti, >750 for Ca and >450 for Al. Ratios of Mg to Li, Ni, Cr and V were >1000. The full procedural Mg blank was less than 5 ng which is negligible compared to 50 µg Mg in the processed samples.

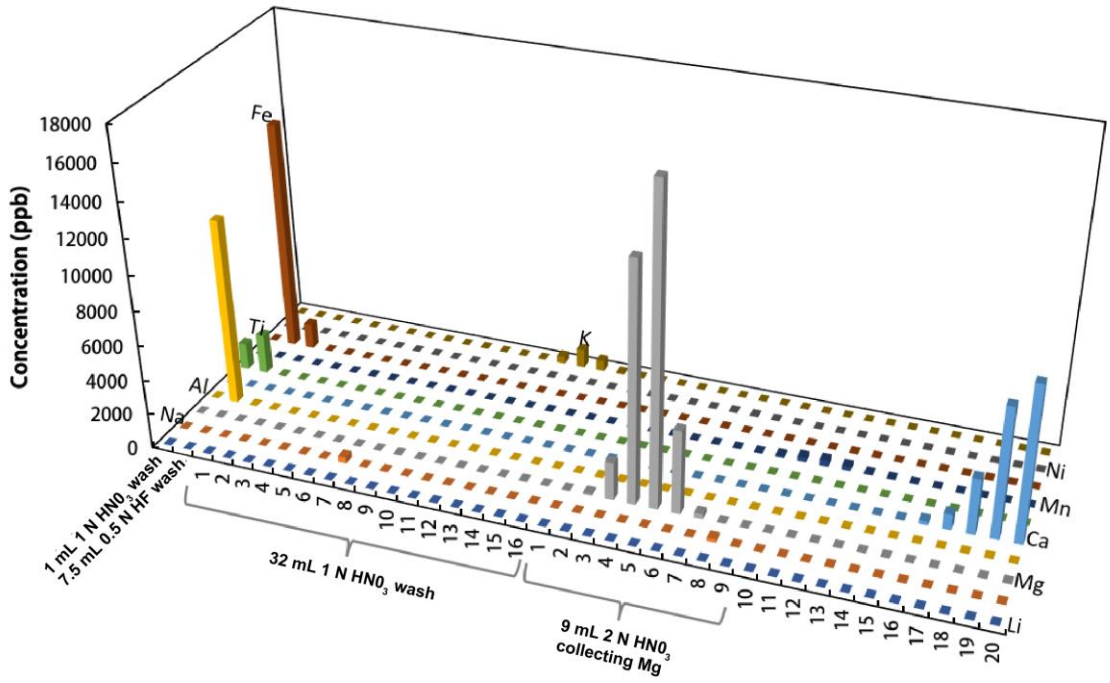

Figure S-4 Elution profile of the first magnesium column separation with 2.5 mL Biorad AG50W-X12 resin. Splits of 1 mL were taken before and after collecting magnesium to monitor the magnesium yield (see Table S-3).

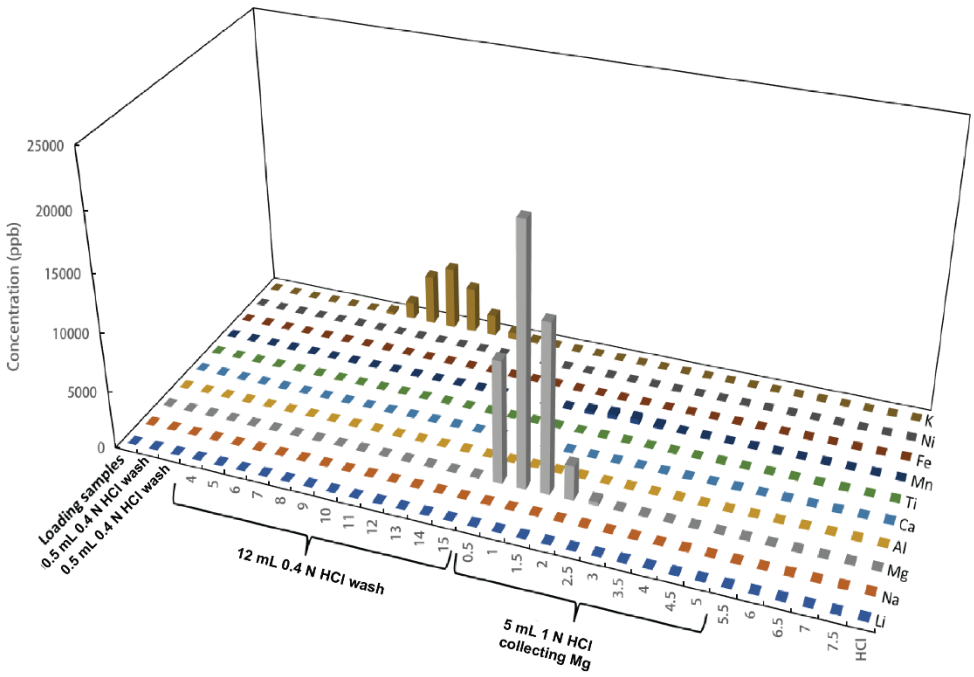

Figure S-5 Elution profile of the second magnesium column separation with 0.25 mL Biorad AG50W-X12 resin. The loaded sample was purified in the first column before loading onto this second column. Splits of 1 mL were taken before and after collecting magnesium to monitor the magnesium yield (see Table S-3).

2.3 Mg isotope analysis

Details of Mg isotope analysis using the critical mixture double-spike method were described by Hin *et al*. (2017). In brief, measurements were performed on a Thermo-Finnigan Neptune (serial no. 1020) multi-collector inductively coupled plasma mass spectrometer (MC-ICPMS) with a combination of Jet sample and H skimmer cones run in medium resolution mode ($M/\Delta M \geq 4000$, 5–95 % peak height definition) following critical double-spiking of all samples (Coath *et al*., 2017). Using a Savillex PFA nebuliser and Apex HF sample introduction system, a 1 μg mL^{-1} Mg sample solution in 2 wt. % HNO_3 yielded intensities of 4×10^{-9} A to 7×10^{-9} A on ^{24}Mg (uptake rate about 40 μL min^{-1}), while the ^{24}Mg intensity of the 'on-peak' blank is lower than 1×10^{-12} A. The data we report for each sample represent the mean of four to eight (usually six) individual runs (*i.e.* each sample run 4–8 times; *N* in Table S-3), each consisting of 20 cycles of 8.4 seconds. An individual run (*i.e.* $N = 1$) consumes about 0.11 μg magnesium. Between every two to three individual sample runs, we make a similar run of a spiked standard. Three individual runs of unspiked DSM-3 were performed at the start, the middle and the end of the sequence to obtain the necessary estimates of the instrumental fractionation factor (Coath *et al*., 2017). A whole sequence containing 10 samples takes about 24 hours.

Mg isotope data are reported against reference standard DSM-3 and uncertainties are two times the standard error of the mean, determined by a homoscedastic approach that pools data of all the standards and samples (Hin *et al*., 2017). Counting statistics dictate that if more data are collected, measurement precision should improve as s.d./$\sqrt{N}$. Consequently, if the precision of our measurements is limited by counting statistics, we are justified in using standard errors of the mean instead of taking a more conservative approach of using the 2 s.d. of sample measurements, as is conventional in sample-standard bracketing (Teng, 2017). A way to test if our approach is valid is to compare the 2 s.e. for a sample based on repeated runs within an individual sequence (*e.g.*, $N = 6$) with the 2 s.d. of that same sample run in sequences over a longer term. This is explored in Fig. S-6, using our BHVO-2 data. We show that the 2 s.e. of ±0.026 ‰ for the mean of $N = 6$ repeats in one analytical session is indistinguishable from the 2 s.d. of ±0.027 ‰ for 16 of such BHVO-2 session means analysed in 16 analytical sessions spread over the course of over one year.

Mg isotope data of olivine-glass pair samples are tabulated in Table S-1, and Mg isotope data of arc lava samples are shown in Table S-5. Three arc samples (LAG4, LAG2 and LAS1) were analysed in duplicate, including sample digestion, column purification, mixing with spikes and mass-spectrometric analysis, and yielded repeat values within the cited 2 s.e. uncertainties (Table S-5). Two international rock standards (BHVO-2 and JP-1) were measured together with other samples in this study and their Mg isotope compositions agree with Hin *et al.* (2017) and the recommended value of Teng (2017) (Table S-5).

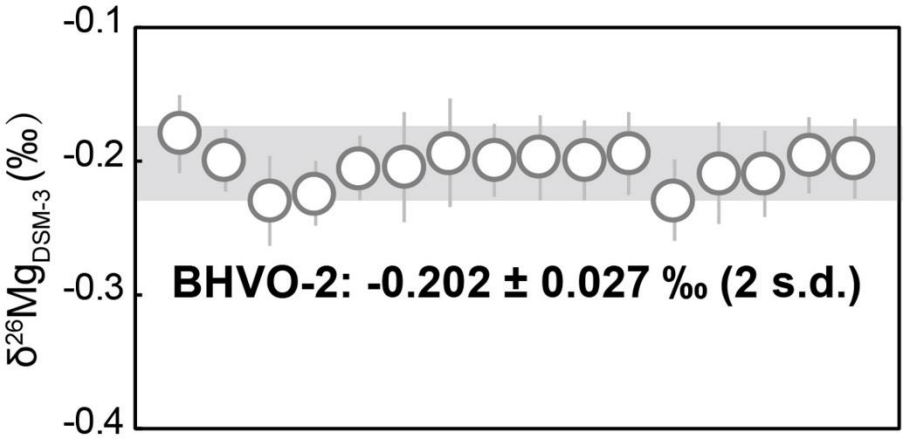

Figure S-6 Long-term variations in the magnesium isotope composition of rock standard BHVO-2, indicating a reproducibility of 0.027 ‰ (2 s.d.).

Table S-3 Mg column chemistry purification protocol. Note that the loading solution contains ~50 µg Mg. The "Mg collection" solution from the 1st column was dried and re-dissolved in 0.4 M HCl for loading onto the 2nd column.

1st column: 2.5 mL Biorad AG50W-X12		2nd column: 0.25 mL Biorad AG50W-X12	
cleaning	6 M HCl, Milli-Q H_2O	cleaning	6 M HCl, Milli-Q H_2O
precondition	4 mL 1 M HNO_3	precondition	1 mL 0.4 M HCl
load sample	0.2 mL 1 M HNO_3	load sample	0.2 mL 0.4 M HCl
wash	2 × 0.5 mL 1 M HNO_3	wash	2 × 0.5 mL 0.4 M HCl
Ti, Al, Fe wash	7.5 mL 0.5 M HF	K wash	11 mL 0.4 M HCl
K wash	31 mL 1 M HNO_3	before-split	1 mL 0.4 M HCl
before-split	1 mL 1 M HNO_3	Mg collection	5 mL 1 M HCl
Mg collection	9 mL 2 M HNO_3	after-split	1 mL 1 M HCl
after-split	1 mL 2 M HNO_3	cleaning	6 M HCl, Milli-Q H_2O
cleaning	6 M HCl, Milli-Q H_2O		

3. Oceanic Arc Lava Samples

3.1 Geological background

The Lesser Antilles arc is formed by the convergence of the Atlantic and Caribbean plates. It extends about 800 km from Grenada in the south to Saba in the north and has been an active volcanic arc since the upper Eocene (Fig. S-7a) (Briden *et al*., 1979). One of the most significant characteristics of this arc is its transition from a typical oceanic arc in the north to a more complex subduction setting in the south (Allen *et al*., 2019). In the north, a package of <1 km of sediments, predominantly pelagic, descends into a clearly defined trench whereas in the south there is a thick (>10 km) accretionary prism, comprised of turbidites derived from the south American craton (Westbrook *et al*., 1984). These abundant sediments play an important role in influencing the trace element composition of magmas in the southern arc (White and Dupré, 1986; van Soest *et al*., 2002; Carpentier *et al*., 2008), although the process by which this occurs is much disputed. The case has been alternatively made for crustal assimilation (Thirlwall and Graham, 1984; Davidson and Harmon, 1989; van Soest *et al*., 2002; Bezard *et al*., 2014) and incorporation of sediment into the mantle sources of the arc lavas (White and Dupré, 1986; van Soest, 2000; Carpentier *et al*., 2008; Labanieh *et al*., 2012; Tang *et al*., 2014).

The Mariana arc is a relatively simple intra-oceanic arc formed by the westward subduction of the Pacific Plate beneath the Philippine Sea Plate (Fig. S-7b), which isolates the present arc from terrigenous material input. A sedimentary package of ~500 m is subducted beneath the arc, which is argued to variably contribute to the magmas of the different islands but not in a systematic manner along arc (*e.g.*, Elliott *et al*., 1997).

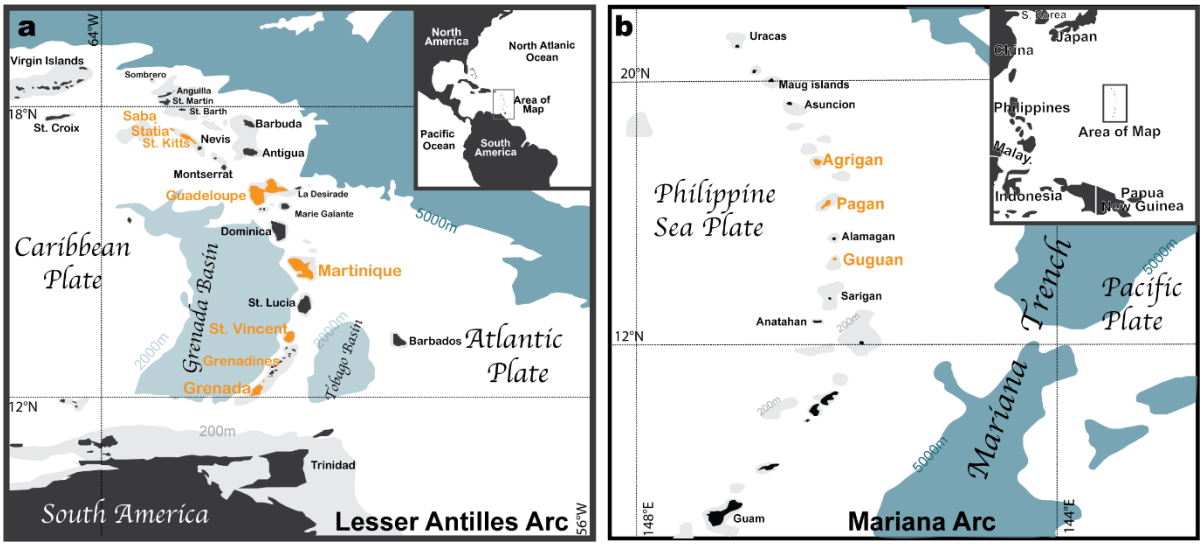

Figure S-7 Maps of **(a)** the Lesser Antilles (after Labanieh *et al*., 2012) and **(b)** the Mariana Trench (after Stewart, 1980) arc systems. The islands highlighted in orange indicate those studied in this work.

3.2 Lesser Antilles samples

Our Lesser Antilles samples have Mg# from 77 to 45 and range from silica undersaturated, high-MgO basalts to basaltic andesites. All samples are porphyritic lavas, except for LAE3 which is a troctolite cumulate xenolith, from Statia. Mineral assemblages of each sample are presented in Table S-7. We analysed 11 arc samples from a suite documented in detail by van Soest (2000) and van Soest *et al*. (2002) and an additional five high-MgO primitive arc basalts from the Lesser Antilles.

A priority of the work by van Soest (2000) was to analyse He isotopic compositions of the lavas. As a result, their sampling focused on the youngest (to avoid post-eruptive He ingrowth) and relatively mafic samples (that contain olivine phenocrysts, which most effectively trap magmatic He). These criteria well suit the aims of our study. Magnesium isotope ratios are readily fractionated by weathering (Teng *et al*., 2010b; Pogge von Strandmann *et al*., 2008), especially in sub-tropical environments such as the Lesser Antilles. Working on the youngest, freshest samples helps guard against potential perturbation by weathering. Equally, analysing mafic samples should minimise changes in the Mg isotope composition that might occur during more complex, late-stage differentiation.

The Lesser Antilles arc is unusual in having examples of plausibly primitive arc basalts (Thirlwall *et al*., 1996; Stamper *et al*., 2014a, 2014b; Melekhova *et al*., 2013, 2015; Camejo-Harry *et al*., 2019). The primitive samples we studied include two picrites from Grenada, AMG6103 (Thirlwall *et al*., 1996) and LAG4 (van Soest, 2000), two high-MgO basalts from St. Vincent, RSV51 and RSV52 (Robertson, 2002), and another one from Kick 'em Jenny (KEJ011-2, Sigurdsson and Shepherd, 1974). Of these five samples, AMG6103 is argued to represent a primary mantle melt parental to more evolved Grenada lavas, as based on petrological experiments (Stamper *et al*., 2014a, 2014b). LAG4 is primitive given its highly forsteritic (Fo up to 90) olivine phenocrysts which are not mantle xenocrysts (given their relatively elevated Ca, see Section 3.7). RSV51 and RSV52 are typical high-MgO basalts from St. Vincent and similar to another St. Vincent basalt (RSV49), which was experimentally determined to be a primary mantle melt (Melekhova *et al*., 2013, 2015): it has a composition consistent with a partial melt of hydrous peridotite at 1.5 GPa, which on differentiation can reproduce the compositions of more evolved magmas found at St. Vincent (Melekhova *et al*., 2013, 2015). The Kick 'em Jenny sample (KEJ011-2) is also argued to represent a primitive arc magma in equilibrium with mantle peridotite (Camejo-Harry *et al*., 2019).

In our more differentiated samples, phenocryst assemblages are usually dominantly comprised of plagioclase and clinopyroxene but in LSS1 oxy-hornblende is the major phenocryst. Olivine phenocrysts are less abundant, typically ~10 % in the more mafic samples (although up to 20 % in LAG4) but more commonly less than 5 % in the more evolved samples.

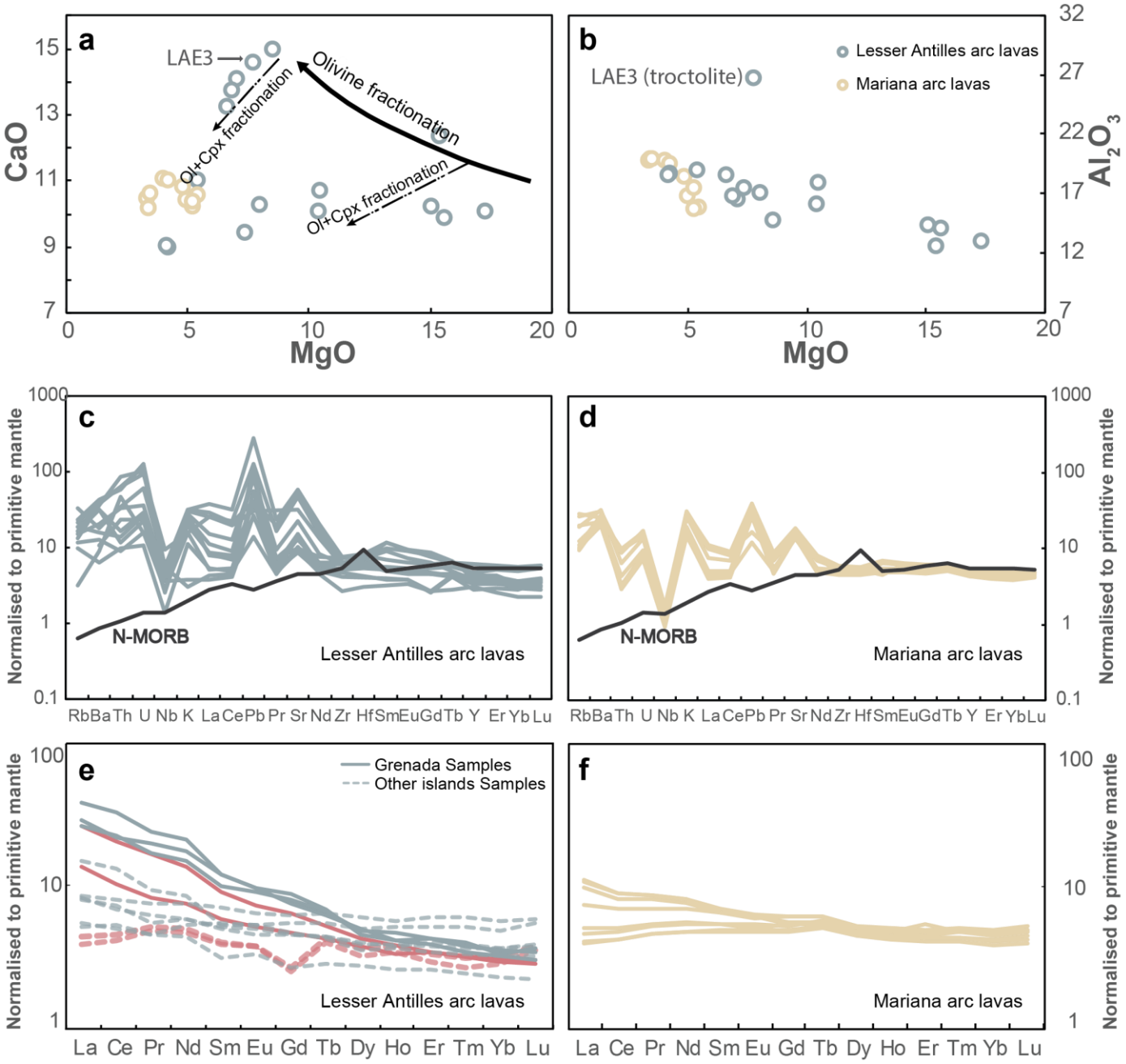

Figure S-8 Compositional variations in Lesser Antilles and Mariana arc lavas used in this study. **(a)** MgO (wt. %) *vs.* CaO (wt. %) and **(b)** MgO (wt. %) *vs.* Al_2O_3 (wt. %). The solid curve in **(a)** represents olivine fractionation from a magma of picritic basalt composition and the dashed curves are vectors for olivine + clinopyroxene fractionation (from Macdonald *et al*., 2000). **(c)** and **(d)** Primitive mantle normalised trace element 'spider diagrams' of Lesser Antilles (KEJ011-2 is not included because of the lack of trace element data) and Mariana samples, respectively. The dark line represents N-MORB, data from Klein (2003). **(e)** Primitive mantle normalised REE distribution pattern of Lesser Antilles samples. The solid lines represent Grenada samples and dashed lines represent samples from the other islands. The REE patterns of four primitive arc magma samples from Grenada (AMG6103 and LAG4) and from St. Vincent (RSV51 and RSV52) are highlighted as solid and dashed red lines, respectively. **(f)** Primitive mantle normalised REE distribution pattern of Mariana samples. All the normalisation values are from Sun and McDonough (1989). In all panels, the data of Lesser Antilles arc lavas are from van Soest (2000), Robertson (2002), Thirlwall *et al*. (1996) and Sigurdsson and Shepherd (1974). The data of Mariana arc lavas are from Elliott *et al*. (1997). A cumulate troctolite sample (LAE3) is highlighted in panels **(a)** and **(b)**.

Figure S-8 highlights some compositional features of our samples. The wide range of MgO contents in our Lesser Antilles lavas helps define their history of differentiation, which will be discussed below in Section 3.8. All Lesser Antilles lavas have clear geochemical signatures of subduction with positive lead and negative niobium anomalies (Fig. S8c). Unusually, Grenada arc lavas, including the two primitive magma samples (AMG6103 and LAG4, highlighted in solid red lines), have steeply inclined REE slopes in Figure S8e, which is indicative of melting in the garnet stability field (Shimizu and Arculus, 1975; van Soest, 2000; Stamper *et al*., 2014a). Most arc lavas from other islands have 'flat' REE patterns (including the two primitive magma samples from St. Vincent of RSV51 and RSV52, highlighted dashed red lines), suggesting these melts were generated at shallow depth where spinel is the stable aluminium-bearing mineral (van Soest, 2000; Stamper *et al*., 2014a).

3.3 Mariana samples

We analysed 10 samples documented in Elliott *et al*. (1997) from Guguan, Pagan and Agrigan in the Central Island Province. The Mariana samples were collected for a U-series study and so are all very young (<10 ka). Moreover, they have ($^{234}U/^{238}U$) activity ratios within error of unity (Elliott *et al*., 1997; Avanzinelli *et al*., 2012), documenting a lack of perturbation by alteration. Our samples are all basaltic andesites with Mg# of 40–50. They show limited variation in MgO *vs*. CaO and Al_2O_3 space (Fig. S-8a, b), which inhibits identifying their differentiation paths. Previous work on Mariana arc lavas and cumulates argued that magmas followed multiple differentiation paths, with major element variations dominantly controlled by crystal fractionation (Woodhead, 1988). In general terms, the Mariana samples lie towards the low MgO end (~4 wt. %) of the liquid lines of descent defined by the Lesser Antilles samples (Fig. S-8a, b). Relative trace element abundances indicate a strong subduction influence (Fig. S-8d). They also have 'flat' primitive mantle normalised REE patterns implying melting in the spinel stability field (Fig. S-8f). While the detailed petrogenesis of Mariana arc lavas is different to the Lesser Antilles, both systems have archetypical characteristics of island arc lavas, reflecting inputs from slightly different subducting assemblages (Plank and Langmuir, 1988).

3.4 Defining the reference δ^{26}Mg value of MORB

Given the limited database of Mg isotope compositions for MORB samples analysed by the critical mixture double-spike method (Hin *et al*., 2017), we use the sample-standard bracketing literature data from Teng *et al*. (2010a) and Bourdon *et al*. (2010) to define a reference δ^{26}Mg value for MORB. There are 51 samples with δ^{26}Mg between −0.17 ± 0.04 ‰ and −0.31 ± 0.07 ‰ (Fig. S-9). The data pass a Shapiro-Wilk test (p = 0.185 for α = 0.05), implying that they are normally distributed, as is also suggested by a normal probability Q-Q plot (Fig. S-10). Thus, we can treat the MORB as a single population and take the weighted mean and error of these 51 data to obtain a mean δ^{26}Mg for MORB of −0.24 ± 0.01 ‰ (2 s.e.). We note that this value agrees well with the three MORB critical mixture double-spike data from Hin *et al*. (2017) and with the three MORB glasses we analysed in this study (Table S-2).

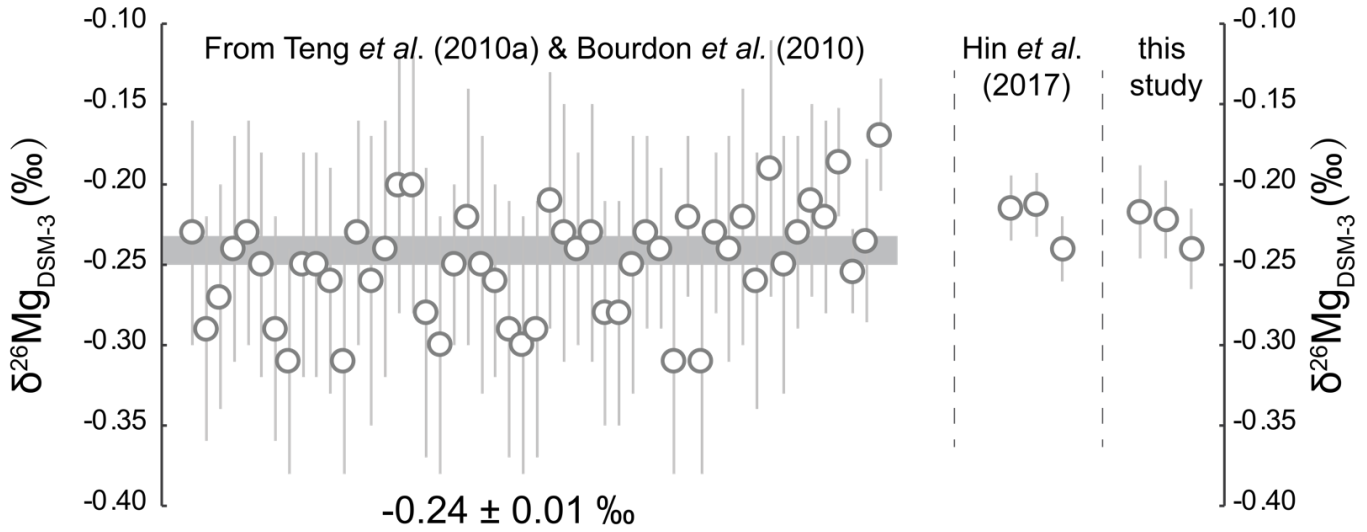

Figure S-9 Literature Mg isotope data of MORB (Teng *et al*., 2010a; Bourdon *et al*., 2010). The grey bar depicts their weighted mean (−0.24 ± 0.01 ‰) calculated from $\sum \frac{\bar{x}}{S^2} / \sum \frac{1}{S^2}$ with variation of $\sqrt{1/\sum \frac{1}{S^2}}$.

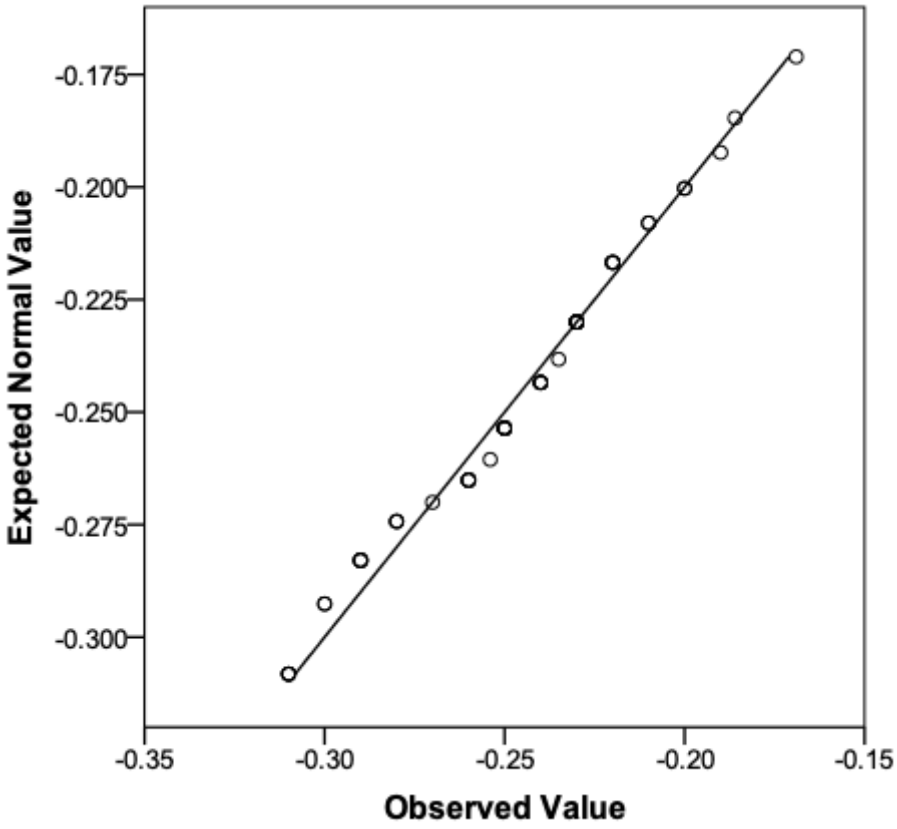

Figure S-10 Normal probability quantile-quantile (Q-Q) plot of 51 literature Mg isotope data of MORB samples. The data lie approximately on a straight line, which suggests they are normally distributed.

3.5 Subduction mixing model

Subducted slab components have variable Mg isotopic compositions, but most variation is restricted to −0.6 ‰ to +0.2 ‰ (Fig. 3a) (Huang *et al*., 2015; Teng *et al*., 2016; Hu *et al*., 2017; Liu *et al*., 2017; Zhong *et al*., 2017; Huang *et al*., 2018). Critical in understanding the influence of these components on the mantle wedge is constraining the amount of Mg transferred from a slab, because the mantle wedge represents a large source of Mg that is difficult to perturb significantly. To this end, we performed binary mixing calculations between mantle and the subduction zone inputs. The input parameters are given in Table S-4 and below we briefly justify some of our choices for these compositions.

In Fig. 3b, H_2O content was chosen to constrain the maximum input of subduction dehydration fluid because its proportion in dehydration fluids is relatively well-constrained (Manning, 2004; Kessel *et al*., 2005; Scambelluri *et al*., 2015; Gervasoni *et al*., 2017) and the depleted mantle is usually anhydrous (*e.g*., Gose *et al*., 2009). Since H_2O contents in primitive arc magmas are less than 10 wt. % (Grove *et al*., 2012), typically ~4 wt. % (Plank *et al*., 2013), and degrees of partial melting are estimated to be about 10–20 % (Plank and Langmuir, 1988; Turner *et al*., 2006), the H_2O content in the mantle source should be less than 2 wt. % (upper limit) because H_2O is highly incompatible (*e.g*., Tenner *et al*., 2009). MgO contents in hydrous melts and fluids are from experimental studies (Manning, 2004; Kessel *et al*., 2005; Scambelluri *et al*., 2015; Gervasoni *et al*., 2017). None of the mixing curves in Fig. 3b have significantly perturbed δ^{26}Mg values with mantle wedge [H_2O] < 2 wt. %.

Some recent studies of Mg isotope compositions in metamorphic rock have invoked that fluids from serpentinite dehydration have MgO as high as 39.8 % (*e.g*., Huang *et al*., 2020). These are the levels of MgO found in peridotites and there is no experimental support for such extremely Mg-rich fluid compositions, so we do not consider them here. Even assuming serpentinite dehydration fluids are implausibly rich in MgO (16.1 wt. %, the value used in the mixing model by Huang *et al*., 2020) and have an extremely high δ^{26}Mg value (~0.95 ‰, the highest value in serpentinite fluid speculated by Chen *et al*., 2016), obtaining δ^{26}Mg as observed in arc lavas still requires 20 % fluid contribution. This would increase the H_2O content in the mantle source of arc lavas to over 10 wt. % (serpentinite dehydration curve in Fig. 3b), which is untenable (Grove *et al*., 2012; Plank *et al*., 2013).

In Fig. 3c, the amount of sediment input is constrained by the Nd isotope ratio because both mantle and primitive melt have distinct Nd isotope ratios compared to sediments (Labanieh *et al*., 2012). The MgO content, Mg isotope ratio and Nd isotope data of subducted sediments follow the parameters used by Teng *et al.* (2016).

3.6 Weathering and melting depth influence on the δ^{26}Mg

Given the mobility of Mg during weathering, potential disturbance of Mg isotope ratios by secondary alteration is an important consideration. Weathered residues typically have elevated δ^{26}Mg as isotopically light Mg is preferentially lost to river systems (Tipper *et al*., 2006; Pogge von Strandmann *et al*., 2008; Teng *et al*., 2010b). To guard against this problem, we selected some of the youngest samples both from the Lesser Antilles and Mariana arc systems, although not all our Lesser Antilles samples are perfectly pristine. We use loss on ignition (LOI) as a rough estimate of the abundance of secondary minerals. In Figure S-11a, it can be seen that there is no systematic relationship between LOI and δ^{26}Mg. Importantly, some of our samples with elevated δ^{26}Mg show some of the lowest LOI, which implies a limited role of secondary alteration in causing the higher δ^{26}Mg value in arc lavas. Samples from the earlier study of Teng *et al*. (2016) range to higher LOI, although again there is no clear relationship with δ^{26}Mg (Fig. S-11b).

The Lesser Antilles are unusual in containing magmas with compositions ranging from alkaline basalts in Grenada to more typical arc lavas further north in the arc. These differences in major element abundances, also linked to contrasting rare earth element patterns (Fig. S-8e), have been attributed to different depths and degrees of melting (Shimizu and Arculus, 1975; van Soest, 2000; Stamper *et al*., 2014a). We can test if this variability in melting process has a significant influence on δ^{26}Mg by comparing our primitive lavas from Grenada and St. Vincent, which span this compositional range. These samples all have indistinguishable and MORB-like δ^{26}Mg regardless of $[La/Yb]_N$. The lack of correlation in Fig. S-12 supports a lack of melting depth effect.

Table S-4 Parameters used in subduction mixing models (see Fig. 3b, c in the main text for results).

	Value	Reference
Hydrous eclogite melt	MgO = 2.5 % H_2O = 15 % $\delta^{26}Mg$ = 0.10 ‰	Gervasoni *et al.* (2017) Gervasoni *et al.* (2017) Wang *et al.* (2020)
Serpentinite dehydration fluid	MgO = 16.1 %, H_2O = 80 % $\delta^{26}Mg$ = 0.95 ‰	Huang *et al.* (2020) Scambelluri *et al.* (2015) Chen *et al.* (2016)
Altered oceanic floor dehydration fluid	MgO = 1 % H_2O = 50 % $\delta^{26}Mg$ = 0.26 ‰	Wang *et al.* (2017) Kessel *et al.* (2005) Wang *et al.* (2017)
Depleted mantle:	MgO = 37.8 % H_2O = 0 % $\delta^{26}Mg$ = –0.240 ‰ $^{143}Nd/^{144}Nd$ = 0.51301 Nd = 0.02 ppm	McDonough and Sun (1995) *e.g.*, Gose *et al.* (2009) Hin *et al.* (2017) Labanieh *et al.* (2012) Labanieh *et al.* (2012)
Subducting sediments	MgO = 2.55 % $\delta^{26}Mg$ = –0.06 ‰ $^{143}Nd/^{144}Nd$ = 0.51181 Nd = 7.9 ppm	Plank (2014) Teng *et al.* (2016) Labanieh *et al.* (2012) Labanieh *et al.* (2012)
Primitive melt end member	MgO = 15 % $\delta^{26}Mg$ = –0.242 ‰ $^{143}Nd/^{144}Nd$ = 0.51301 Nd = 1.34 ppm	Mean of five primitive samples, this study Mean of five primitive samples, this study Labanieh *et al.* (2012) Labanieh *et al.* (2012)

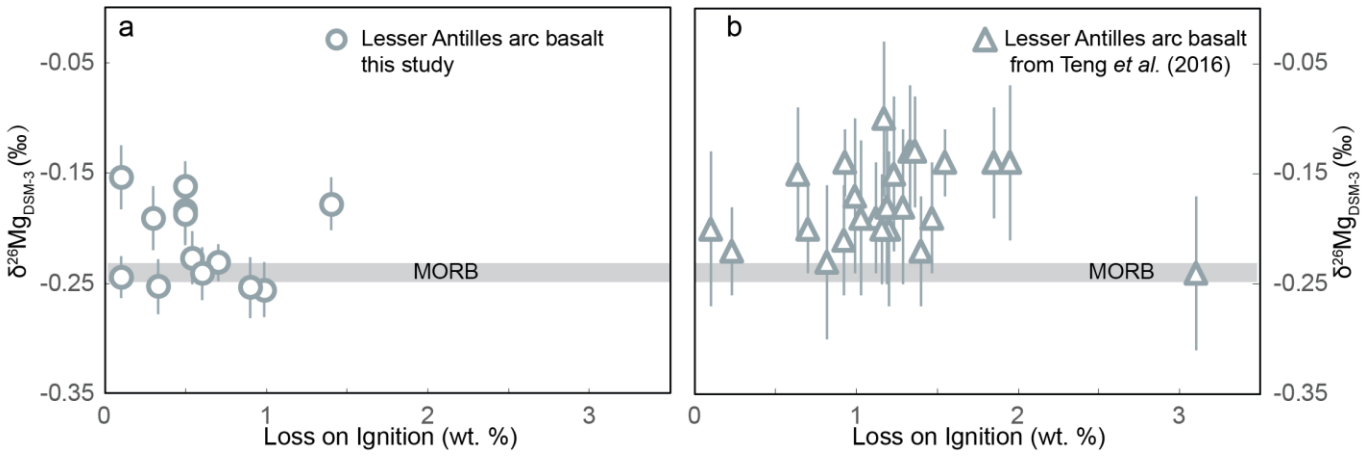

Figure S-11 (a) Loss on Ignition (LOI) against $\delta^{26}Mg$ for Lesser Antilles samples of this study (no available LOI data for LAE3, LAV2 and KEJ011-2). Values for LOI are not available for the Mariana samples but none of their major element totals differ from 100 % by more than 0.5 % (Elliott *et al.*, 1997) indicating comparably low LOI. **(b)** LOI against $\delta^{26}Mg$ of Lesser Antilles samples from Teng *et al*. (2016). The grey bar represents the mean Mg isotope ratio of MORB reference (−0.24 ± 0.01 ‰).

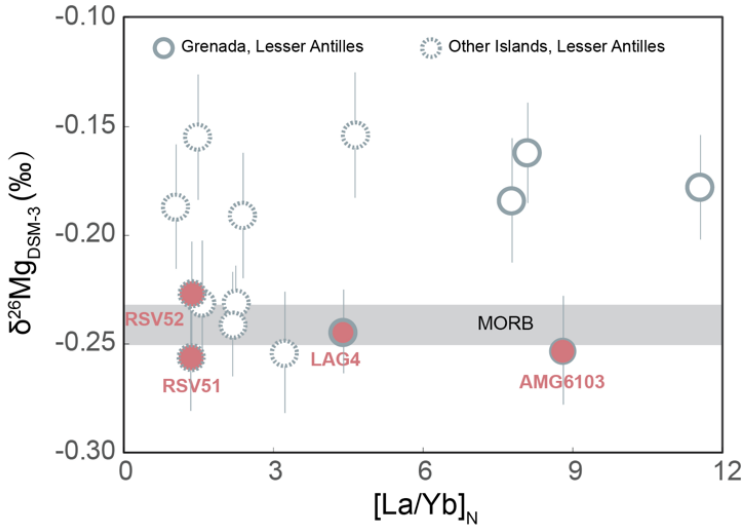

Figure S-12 Plots of primitive mantle normalised La/Yb ratio *vs.* δ^{26}Mg of Lesser Antilles samples (trace element data for KEJ011-2 is not available). Solid circles represent Grenada samples, dashed circles are samples from other islands. Primitive samples are highlighted in red (LAG4 and AMG6103 from Grenada; RSV51 and RSV52 from St. Vincent).

3.7 Olivine phenocrysts in Lesser Antilles samples

Given the important role of olivine on the Mg budget of lavas, we analysed the olivine compositions of a representative set of olivine bearing samples from the Lesser Antilles (full set of analyses reported in Table S7). These analyses provide important information on the origin of the olivine crystals in the different petrographic groups (primitive, xeno, evolved and cumulate), identified in the main text.

The compositions of primitive olivines are defined by the analyses of the sample LAG4. LAG4 has abundant olivine phenocrysts (~20 %) and its bulk chemical composition is similar with the other primitive samples (*i.e.* RSV51, RSV51, KEJ011-2, and AMG6103) (Sigurdsson and Shepherd, 1974; Thirlwall *et al.*, 1996; van Soest 2000; Robertson, 2002). The bulk sample chips of other primitive samples were not available. These olivines from LAG4 are Fo- and Ni-rich but have 0.1–0.3 wt. % CaO, implying they are a result of magmatic crystallisation rather than mantle xenocrysts. Olivine crystals from three samples in the 'Xeno' group (WIC19, LSS1 and LAS1) are similarly Fo- and Ni-rich, yet the bulk lavas are more differentiated and have lower bulk Mg# (~64 to 70) than the primitive samples (~77) (Table S-5). In the one thin section we have of these samples (see Fig. 4b), LSS1 shows a typical reaction relationship between olivine and groundmass. Such textural and chemical evidence for disequilibrium argues that olivine crystals in WIC19, LSS1 and LAS1 samples (*i.e.* the 'Xeno' samples) are entrained, xenocrystic, cumulate olivines (*i.e.* magmatic; Fig. S-13a) rather than phenocrysts from its host magma. Olivine analyses of all other, more evolved samples (including troctolite cumulate LAE3) have olivines with a wide range of lower Fo, relatively high CaO and low NiO (Fig. S-13).

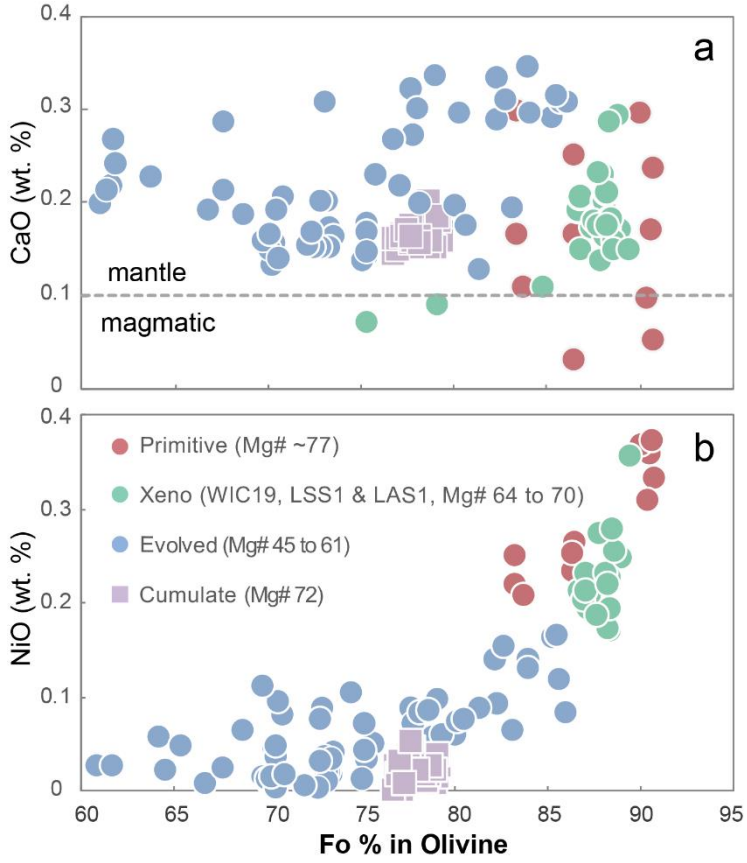

Figure S-13 Electron microprobe data of olivine crystals in Lesser Antilles samples. Plotted with Fo *vs*. **(a)** CaO content and **(b)** NiO content. See Table S-7 for data.

3.8 The liquid line of descent of Lesser Antilles arc lavas

To model Mg isotope fractionation during magmatic differentiation, we need to determine the liquid line of descent of the magmas. Considering the complicated differentiation history of many arc lavas, we focus on the early differentiation stage, which is possible in the Lesser Antilles case due to the presence of primitive arc lavas in this location. We initially consider the samples from Grenada, where magmatic differentiation has been studied in detail (*e.g.*,Thirlwall *et al.*, 1996; Macdonald *et al.*, 2000; Stamper *et al.*, 2014a, 2014b). Two differentiation series have been identified (C-series and M-series), which are evident on a plot of MgO *vs*. CaO (Fig. S-14a). M-series basalts from Grenada differentiated under high pressure conditions (P > 1.3 GPa, Stamper *et al.*, 2014b), which resulted in cocrystallisation of olivine and clinopyroxene and consequently decreases in both Mg and Ca in the evolving magma. C-series basalts are relatively CaO-enriched and experimental petrology suggests that C-series basalts result from low pressure crystallisation where the olivine stability field is expanded relative to clinopyroxene (Stamper *et al.*, 2014b), resulting in increasing CaO contents in the melt as it evolves until clinopyroxene crystallisation sets in. As shown in Fig. S-14a, our three differentiated Grenada lavas (LAG2, LSG5 and LSG8, "Evolved" group) are typical of the most Ca-enriched basalts of the C-series. Experiments show such magmas are formed by removal of ~20 % olivine and minor spinel as the only liquidus phases from a primitive magma (Stamper *et al.*, 2014b).

Similar differentiation paths under polybaric condition are also identified in both Bequis and St. Vincent Island of Lesser Antilles (Tollan *et al.*, 2012; Melekhova *et al.*, 2015; Camejo-Harry *et al.*, 2018). Studies of other Lesser Antilles islands do not clearly identify two liquid lines of descent like the C- and M-series, but still argue that crystallisation of olivine and clinopyroxene accounts for petrological observations (Cooper *et al.*, 2016; Melekhova *et al.*, 2017). This is also evident in the MgO *vs*. CaO plots (Fig. S-14b). The trends evident in the C- and M-series defined

in Grenada can been seen more generally in all Lesser Antilles lavas where C-series corresponds to the Ol crystallisation (simplified as "Ol line") and M-series corresponds to the Ol + Cpx crystallisation (simplified as "Ol + Cpx line") (Fig. S-14b).

Our "Evolved" samples lie after the CaO inflection point of the Ol line (two samples with lowest MgO may belong to the Ol + Cpx line trend, but this is not well-distinguished for the low MgO samples). The three "Xeno" samples (WIC19, LSS1, LAS1) appear to lie on Ol + Cpx line trend. As discussed in the main text and Section 3.7 above, the three "Xeno" samples have xenocrystic olivine phenocrysts (Figs. 4b, S-13). Therefore, we propose that rather than having evolved from primitive lavas through olivine + clinopyroxene crystallisation, the three "Xeno" samples have been produced by adding primitive cumulate olivine to more differentiated lavas, as shown in Fig. S-14b. We are not arguing that all the samples on the Ol + Cpx line are derived from adding cumulate olivine to more evolved samples, as petrographic and experimental studies strongly support cocrystallisation of olivine and clinopyroxene in producing M-series lavas (*e.g.*, Thirlwall *et al.*, 1996; Macdonald *et al.*, 2000; Stamper *et al.*, 2014a, 2014b). Yet the petrographic and geochemical observations (Fig. 4b, Fig. S-13) in our three "Xeno" samples make a clear case for olivine accumulation in these samples, causing coincidental overlap with the Ol + Cpx line trend.

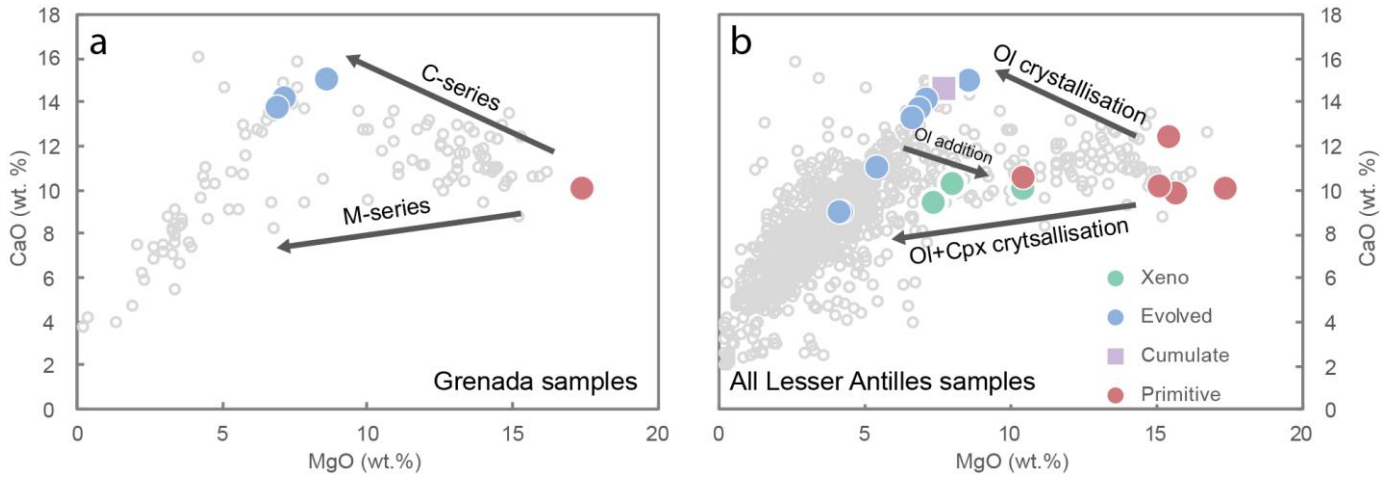

Figure S-14 (a) CaO *vs*. MgO of Grenada samples. Background grey dots are Grenada samples from literature (online GEOREC database). Grey dots define two liquid lines of descent, C-series and M-series. **(b)** CaO *vs*. MgO of all Lesser Antilles samples, which show similar differentiation trends to Grenada C-series (Ol crystallisation) and M-series (Ol + Cpx crystallisation). An olivine addition arrow indicates a mechanism through which 'Xeno' samples could be produced.

3.9 The Mg isotope fractionation during magma differentiation modelling

We set the initial δ^{26}Mg of the primitive magma as −0.242 ‰, which is the average value of measured Mg isotope ratios of five primitive magma samples. We use a primitive MgO content of 15 wt. % (also the average MgO content of our five primitive magma samples). We calculated two differentiation paths, co-crystallisation of 20 % olivine and 20 % clinopyroxene and 20 % Ol-only fractionation to represent both endmember liquid lines of descent. The percentages of crystallisation are based on the experimental study of Stamper *et al.* (2014b). We used the following equations (modified after DePaolo, 1981) to describe fractional crystallisation:

$$c_l^i = c_0^i F^{D_i - 1}$$

$$\delta^{26}\mathrm{Mg}_{\text{residual melt}} = \delta^{26}\mathrm{Mg}_{\text{initial}} + 1000\, D_i \ln(F) \ln({}^{26/24}\alpha_{\text{solid/melt}})$$

c_l^i and c_0^i are MgO contents in residual and initial melts; F is the liquid mass fraction; D_i is Mg distribution coefficient between the solid phase and melt (4.44 for olivine-melt, Beattie, 1994; 2.11 for Cpx-melt, Adam and Green, 2006).

$^{26/24}\alpha_{solid/melt} = \exp[(\Delta^{26/24}Mg_{solid/melt})/1000]$. $\Delta^{26/24}Mg_{Ol/melt} = -0.071$ ‰ (1438 K, this study). $\Delta^{26/24}Mg_{Cpx/melt}$ (0.039 ‰) is calculated from $\Delta^{26/24}Mg_{Cpx/Ol} + \Delta^{26/24}Mg_{Ol/melt}$, where $\Delta^{26/24}Mg_{Cpx/Ol}$ (0.11 ‰) is from the average of literature data (Handler *et al.*, 2009; Yang *et al.*, 2009; Huang *et al.*, 2011; Liu *et al.*, 2011; Pogge van Strandmann *et al.*, 2011; Xiao *et al.*, 2013, 2016; Lai *et al.*, 2015; Liu *et al.*, 2017; Stracke *et al.*, 2018). Given the dominant control of olivine on removal of Mg from the evolving liquid and its greater fractionation relative to melt compared to clinopyroxene, the calculations are most strongly controlled by our new value of $\Delta^{26/24}Mg_{Ol/melt}$.

In keeping with the earlier discussion, the "Xeno" samples were modelled with olivine accumulation (Fig. 4d). Composition of the accumulated olivine: MgO of 45 % and δ^{26}Mg of −0.313 ‰ (olivine crystallised from primitive melt whose δ^{26}Mg is −0.242 ‰ and considering $\Delta^{26/24}Mg_{Ol/melt}$ of −0.071 ‰).

Table S-5 Magnesium isotope ratios of Lesser Antilles and Mariana arc lavas.

	$\delta^{26}Mg_{DSM-3}$ (‰)	Pooled 2 s.e.	*N*	MgO (wt. %)	Mg#	Grouping	Location
Lesser Antilles arc basalts							
LAG4	−0.245	0.030	8	17.31	77.4	Primitive	Grenada
rpt	−0.244	0.024	8				
mean	*−0.245*	*0.019*	*16*				
RSV51*	−0.256	0.025	8	15.61	75.25	Primitive	St. Vincent
RSV52*	−0.227	0.024	8	15.06	74.85	Primitive	St. Vincent
KEJ011-2*	−0.231	0.030	6	10.46	73.64	Primitive	Grenadines
AMG6103*	−0.253	0.025	8	15.28	73.79	Primitive	Grenada
WIC19	−0.254	0.028	6	10.40	70.53	Xeno	Grenadines
LSS1	−0.241	0.024	4	7.37	63.89	Xeno	Saba
LAS1	−0.230	0.021	5	8.01	66.01	Xeno	Saba
rpt	*−0.232*	*0.024*	*8*				
mean	*−0.231*	*0.017*	*13*				
LSG8	−0.184	0.029	8	7.06	56.82	Evolved	Grenada
LSG5	−0.178	0.024	4	8.55	61.62	Evolved	Grenada
LAG2	−0.142	0.030	8	6.86	55.77	Evolved	Grenada
rpt	*−0.189*	*0.036*	*6*				
mean	*−0.162*	*0.023*	*14*				
LAV2	−0.155	0.029	8	4.15	47.67	Evolved	St. Vincent
LSMO7	−0.154	0.029	8	5.39	53.95	Evolved	Martinique
GUAD511	−0.191	0.029	8	6.61	54.65	Evolved	Guadeloupe
LSK2	−0.187	0.029	8	4.20	45.21	Evolved	St. Kitts
LAE3	−0.231	0.029	8	7.72	72.25	Cumulate	Statia
Mariana arc basalts							
AGR2	−0.106	0.022	6	4.98	44.21		Agrigan
AGR4b	−0.139	0.030	4	4.80	46.18		Agrigan
PAG1	−0.112	0.022	6	5.45	46.97		Pagan
PAG3	−0.139	0.022	6	5.25	45.96		Pagan
GUG3	−0.164	0.031	6	3.36	40.13		Guguan
GUG4	−0.188	0.031	6	5.22	50.20		Guguan
GUG6	−0.155	0.031	6	3.99	44.15		Guguan
GUG9	−0.172	0.031	6	4.23	45.42		Guguan
GUG11	−0.154	0.031	6	3.38	41.81		Guguan
GUG13	−0.174	0.031	6	3.47	41.55		Guguan
Rock standards							
BHVO-2	−0.202	0.008	81				
JP-1	−0.221	0.016	23				

MgO and Mg# data of Lesser Antilles arc lavas are from van Soest (2000) except samples labelled with an asterisk (*), which are from Thirlwall *et al*. (1996), Robertson (2002), and Sigurdsson and Shepherd (1974). Mariana arc lavas are from Elliott *et al*. (1997).
rpt refers to a repetition of the whole chemical and analytical process, including digestion, column chemistry and instrument analysis.

Supplementary Tables (as Excel files)

Table S-6 Microprobe data and BSE images of the olivine and glass of olivine-glass pair samples.

Table S-7 Mineral assemblages and microprobe data of olivine in Lesser Antilles samples.

Tables S-6 and S-7 are available for download (Excel) from the online version of the article at https://doi.org/10.7185/geochemlet.2226.

Supplementary Information References

Adam, J., Green, T. (2006) Trace element partitioning between mica-and amphibole-bearing garnet lherzolite and hydrous basanitic melt: 1. Experimental results and the investigation of controls on partitioning behaviour. *Contributions to Mineralogy and Petrology* 152, 1–17. https://doi.org/10.1007/s00410-006-0085-4

Allen, R., Collier, J., Stewart, A., Henstock, T., Goes, S., Rietbrock, A., Team, V. (2019) The role of arc migration in the development of the Lesser Antilles: A new tectonic model for the Cenozoic evolution of the eastern Caribbean. *Geology* 47, 891–895. https://doi.org/10.1130/G46708.1

Avanzinelli, R., Prytulak, J., Skora, S., Heumann, A., Koetsier, G., Elliott, T. (2012) Combined ^{238}U–^{230}Th and ^{235}U–^{231}Pa constraints on the transport of slab-derived material beneath the Mariana Islands. *Geochimica et Cosmochimica Acta* 92, 308–328. https://doi.org/10.1016/j.gca.2012.06.020

Beattie, P. (1994) Systematics and energetics of trace-element partitioning between olivine and silicate melts: Implications for the nature of mineral/melt partitioning. *Chemical Geology* 117, 57–71. https://doi.org/10.1016/0009-2541(94)90121-X

Bezard, R., Davidson, J.P., Turner, S., Macpherson, C.G., Lindsay, J.M., Boyce, A.J. (2014) Assimilation of sediments embedded in the oceanic arc crust: myth or reality? *Earth and Planetary Science Letters* 395, 51–60. https://doi.org/10.1016/j.epsl.2014.03.038

Birner, S.K., Cottrell, E., Warren, J.M., Kelley, K.A., Davis, F.A. (2018) Peridotites and basalts reveal broad congruence between two independent records of mantle f_{O2} despite local redox heterogeneity. *Earth and Planetary Science Letters* 494, 172–189. https://doi.org/10.1016/j.epsl.2018.04.035

Bourdon, B., Van Orman, J.A. (2009) Melting of enriched mantle beneath Pitcairn seamounts: Unusual U–Th–Ra systematics provide insights into melt extraction processes. *Earth and Planetary Science Letters* 277, 474–481. https://doi.org/10.1016/j.epsl.2008.11.017

Bourdon, B., Tipper, E.T., Fitoussi, C., Stracke, A. (2010) Chondritic Mg isotope composition of the Earth. *Geochimica et Cosmochimica Acta* 74, 5069–5083. https://doi.org/10.1016/j.gca.2010.06.008

Briden, J.C., Rex, D.C., Faller, A.M., Tomblin, J.F. (1979) K-Ar geochronology and paleomagnetism of volcanic rocks in the Lesser Antilles Island arc. *Philosophical Transactions of the Royal Society. Series A, Mathematical and Physical Sciences* 291, 485–528. https://doi.org/10.1098/rsta.1979.0040

Camejo-Harry, M., Melekhova, E., Blundy, J., Attridge, W., Robertson, R., Christopher, T. (2018) Magma evolution beneath Bequia, Lesser Antilles, deduced from petrology of lavas and plutonic xenoliths. *Contributions to Mineralogy and Petrology* 173, 77. https://doi.org/10.1007/s00410-018-1504-z

Camejo-Harry, M., Melekhova, E., Blundy, J., Robertson, R. (2019) Evolution in magma storage conditions beneath Kick-'em-Jenny and Kick-'em-Jack submarine volcanoes, Lesser Antilles arc. *Journal of Volcanology and Geothermal Research* 373, 1–22. https://doi.org/10.1016/j.jvolgeores.2019.01.023

Carpentier, M., Chauvel, C., Mattielli, N. (2008) Pb–Nd isotopic constraints on sedimentary input into the Lesser Antilles arc system. *Earth and Planetary Science Letters* 272, 199–211. https://doi.org/10.1016/j.epsl.2008.04.036

Chen, Y.-X., Schertl, H.-P., Zheng, Y.-F., Huang, F., Zhou, K., Gong, Y.-Z. (2016) Mg–O isotopes trace and the origin of Mg-rich fluids in the deeply subducted continental crust of Western Alps. *Earth and Planetary Science Letters* 456, 157–167. https://doi.org/10.1016/j.epsl.2016.09.010

Coath, C.D., Elliott, T., Hin, R.C. (2017) Double-spike inversion for three-isotope systems. *Chemical Geology* 451, 78–89. https://doi.org/10.1016/j.chemgeo.2016.12.025

Cooper, G.F., Davidson, J.P., Blundy, J.D. (2016) Plutonic xenoliths from Martinique, Lesser Antilles: evidence for open system processes and reactive melt flow in island arc crust. *Contributions to Mineralogy and Petrology* 171, 87. https://doi.org/10.1007/s00410-016-1299-8

Cottrell, E., Kelley, K.A. (2014) Redox Heterogeneity of the Mantle Inferred from Hotspots. *American Geophysical Union, Fall Meeting 2014*, Abstract V23G-02.

Dauphas, N., Teng, F.-Z., Arndt, N.T. (2010) Magnesium and iron isotopes in 2.7 Ga Alexo komatiites: Mantle signature, no evidence for Soret diffusion, and identification of diffusive transport in zoned olivine. *Geochimica et Cosmochimica Acta* 74, 3274–3291. https://doi.org/10.1016/j.gca.2010.02.031

Davidson, J.P., Harmon, R.S. (1989) Oxygen isotope constrains on the petrogenesis of volcanic arc magma from Martinque, Lesser Antilles. *Earth and Planetary Science Letters* 95, 255–270. https://doi.org/10.1016/0012-821X(89)90101-5

DePaolo, D.J. (1981) Trace element and isotopic effects of combined wallrock assimilation and fractional crystallization. *Earth and Planetary Science Letters* 53, 189–202. https://doi.org/10.1016/0012-821X(81)90153-9

Devey, C.W., Garbe-Schönberg, C.D., Stoffers, P., Chauvel, C., Mertz, D.F. (1994) Geochemical effects of dynamic melting beneath ridges: Reconciling major and trace element variations in Kolbeinsey (and global) mid-ocean ridge basalt. *Journal of Geophysical Research: Solid Earth* 99, 9077–9095. https://doi.org/10.1029/93JB03364

Elliott, T., Plank, T., Zindler, A., White, W., Bourdon, B. (1997) Element transport from slab to volcanic front at the Mariana arc. *Journal of Geophysical Research: Solid Earth* 102, 14991–15019. https://doi.org/10.1029/97JB00788

Gallagher, K., Elliott, T. (2009) Fractionation of lithium isotopes in magmatic systems as a natural consequence of cooling. *Earth and Planetary Science Letters* 278, 286–296. https://doi.org/10.1016/j.epsl.2008.12.009

Gervasoni, F., Klemme, S., Rohrbach, A., Griltzner, T., Berndt, J. (2017) Experimental constraints on mantle metasomatism caused by silicate and carbonate melts. *Lithos* 282–283, 173–186. https://doi.org/10.1016/j.lithos.2017.03.004

Gose, J., Schmädicke, E., Beran, A. (2009) Water in enstatite from Mid-Atlantic Ridge peridotite: Evidence for the water content of suboceanic mantle? *Geology* 37, 543–546. https://doi.org/10.1130/G25558A.1

Graham, D.W., Castillo, P.R., Lupton, J.E., Batiza, R. (1996) Correlated He and Sr isotope ratios in South Atlantic near-ridge seamounts and implications for mantle dynamics. *Earth and Planetary Science Letters* 144, 491–503. https://doi.org/10.1016/S0012-821X(96)00172-0

Grove, T.L., Till, C.B., Krawczynski, M.J. (2012) The Role of H_2O in Subduction Zone Magmatism. *Annual Review of Earth and Planetary Sciences* 40, 413–439. https://doi.org/10.1146/annurev-earth-042711-105310

Handler, M.R., Baker, J.A., Schiller, M., Bennett, V.C., Yaxley, G.M. (2009) Magnesium stable isotope composition of Earth's upper mantle. *Earth and Planetary Science Letters* 282, 306–313. https://doi.org/10.1016/j.epsl.2009.03.031

Hekinian, R., Cheminée, J.L., Dubois, J., Stoffers, P., Scott, S., Guivel, C., Garbe-Schönberg, D., Devey, C., Bourdon, B., Lackschewitz, K., McMurtry, G., Le Drezen, E. (2003) The Pitcairn hotspot in the South Pacific: distribution and composition of submarine volcanic sequences. *Journal of Volcanology and Geothermal Research* 121, 219–245. https://doi.org/10.1016/S0377-0273(02)00427-4

Helz, R.T., Cottrell, E., Brounce, M.N., Kelley, K.A. (2017) Olivine-melt relationships and syneruptive redox variations in the 1959 eruption of Kīlauea Volcano as revealed by XANES. *Journal of Volcanology and Geothermal Research* 333–334, 1–14. https://doi.org/10.1016/j.jvolgeores.2016.12.006

Hin, R.C., Coath, C.D., Carter, P.J., Nimmo, F., Lai, Y.-J., Pogge von Strandmann, P.A.E., Willbold, M., Leinhardt, Z.M., Walter, M.J., Elliott, T. (2017) Magnesium isotope evidence that accretional vapour loss shapes planetary compositions. *Nature* 549, 511–515. https://doi.org/10.1038/nature23899

Hu, Y., Teng, F.-Z., Plank, T., Huang, K.-J. (2017) Magnesium isotopic composition of subducting marine sediments. *Chemical Geology* 466, 15–31. https://doi.org/10.1016/j.chemgeo.2017.06.010

Huang, F., Zhang, Z., Lundstrom, C.C., Zhi, X. (2011) Iron and magnesium isotopic compositions of peridotite xenoliths from Eastern China. *Geochimica et Cosmochimica Acta* 75, 3318–3334. https://doi.org/10.1016/j.gca.2011.03.036

Huang, J., Ke, S., Gao, Y., Xiao, Y., Li, S. (2015) Magnesium isotopic compositions of altered oceanic basalts and gabbros from IODP site 1256 at the East Pacific Rise. *Lithos* 231, 53–61. https://doi.org/10.1016/j.lithos.2015.06.009

Huang, J., Guo, S., Jin, Q.-Z., Huang, F. (2020) Iron and magnesium isotopic compositions of subduction-zone fluids and implications for arc volcanism. *Geochimica et Cosmochimica Acta* 278, 376–391. https://doi.org/10.1016/j.gca.2019.06.020

Huang, K.-J., Teng, F.-Z., Plank, T., Staudigel, H., Hu, Y., Bao, Z.-Y. (2018) Magnesium isotopic composition of altered oceanic crust and the global Mg cycle. *Geochimica et Cosmochimica Acta* 238, 357–373. https://doi.org/10.1016/j.gca.2018.07.011

Jeffcoate, A.B., Elliott, T., Kasemann, S.A., Ionov, D., Cooper, K., Brooker, R. (2007) Li isotope fractionation in peridotites and mafic melts. *Geochimica et Cosmochimica Acta* 71, 202–218. https://doi.org/10.1016/j.gca.2006.06.1611

Kessel, R., Schmidt, M.W., Ulmer, P., Pettke, T. (2005) Trace element signature of subduction-zone fluids, melts and supercritical liquids at 120–180 km depth. *Nature* 437, 724–727. https://doi.org/10.1038/nature03971

Klein, E.M. (2003) 3.13 - Geochemistry of the Igneous Oceanic Crust. In Holland, H.D., Turekian, K.K. (Eds.) *Treatise on Geochemistry*. Third Edition, Elsevier, Amsterdam, 433–463. https://doi.org/10.1016/B0-08-043751-6/03030-9

Labanieh, S., Chauvel, C., Germa, A., Quidelleur, X. (2012) Martinique: a Clear Case for Sediment Melting and Slab Dehydration as a Function of Distance to the Trench. *Journal of Petrology* 53, 2441–2464. https://doi.org/10.1093/petrology/egs055

Lai, Y.-J., Pogge von Strandmann, P.A.E., Dohmen, R., Takazawa, E., Elliott, T. (2015) The influence of melt infiltration on the Li and Mg isotopic composition of the Horoman Peridotite Massif. *Geochimica et Cosmochimica Acta* 164, 318–332. https://doi.org/10.1016/j.gca.2015.05.006

Lesher, C.E., Walker, D. (1986) Solution properties of silicate liquids from thermal diffusion experiments. *Geochimica et Cosmochimica Acta* 50, 1397–1411. https://doi.org/10.1016/0016-7037(86)90313-3

Li, W.-Y., Teng, F.-Z., Xiao, Y., Huang, J. (2011) High-temperature inter-mineral magnesium isotope fractionation in eclogite from the Dabie orogen, China. *Earth and Planetary Science Letters* 304, 224–230. https://doi.org/10.1016/j.epsl.2011.01.035

Liu, P.-P., Teng, F.-Z., Dick, H.J.B., Zhou, M.-F., Chung, S.-L. (2017) Magnesium isotopic composition of the oceanic mantle and oceanic Mg cycling. *Geochimica et Cosmochimica Acta* 206, 151–165. https://doi.org/10.1016/j.gca.2017.02.016

Liu, S.-A., Teng, F.-Z., Yang, W., Wu, F.-Y. (2011) High-temperature inter-mineral magnesium isotope fractionation in mantle xenoliths from the North China craton. *Earth and Planetary Science Letters* 308, 131–140. https://doi.org/10.1016/j.epsl.2011.05.047

Macdonald, R., Hawkesworth, C.J., Heath, E. (2000) The Lesser Antilles volcanic chain: a study in arc magmatism. *Earth Science Reviews* 49, 1–76. https://doi.org/10.1016/S0012-8252(99)00069-0

Manning, C.E. (2004) The chemistry of subduction-zone fluids. *Earth and Planetary Science Letters* 223, 1–16. https://doi.org/10.1016/j.epsl.2004.04.030

McDonough, W.F., Sun, S.-s. (1995) The composition of the Earth. *Chemical Geology* 120, 223–253. https://doi.org/10.1016/0009-2541(94)00140-4

Melekhova, E., Annen, C., Blundy, J. (2013) Compositional gaps in igneous rock suites controlled by magma system heat and water content. *Nature Geoscience* 6, 385–390. https://doi.org/10.1038/ngeo1781

Melekhova, E., Blundy, J., Robertson, R., Humphreys, M.C.S. (2015) Experimental Evidence for Polybaric Differentiation of Primitive Arc Basalt beneath St. Vincent, Lesser Antilles. *Journal of Petrology* 56, 161–192. https://doi.org/10.1093/petrology/egu074

Melekhova, E., Blundy, J., Martin, R., Arculus, R., Pichavant, M. (2017) Petrological and experimental evidence for differentiation of water-rich magmas beneath St. Kitts, Lesser Antilles. *Contributions to Mineralogy and Petrology* 172, 98. https://doi.org/10.1007/s00410-017-1416-3

Niu, Y., Batiza, R. (1994) Magmatic processes at a slow spreading ridge segment: 26°S Mid-Atlantic Ridge. *Journal of Geophysical Research: Solid Earth* 99, 19719–19740. https://doi.org/10.1029/94JB01663

Oeser, M., Dohmen, R., Horn, I., Schuth, S., Weyer, S. (2015) Processes and time scales of magmatic evolution as revealed by Fe–Mg chemical and isotopic zoning in natural olivines. *Geochimica et Cosmochimica Acta* 154, 130–150. https://doi.org/10.1016/j.gca.2015.01.025

Parkinson, I.J., Hammond, S.J., James, R.H., Rogers, N.W. (2007) High-temperature lithium isotope fractionation: Insights from lithium isotope diffusion in magmatic systems. *Earth and Planetary Science Letters* 257, 609–621. https://doi.org/10.1016/j.epsl.2007.03.023

Pickering, J.M., Schwab, B.E., Johnston, A.D. (1998) Off-center hot spots: Double thermocouple determination of the thermal gradient in a 1.27 cm (1/2 in.) CaF_2 piston–cylinder furnace assembly. *American Mineralogist* 83, 228–235. https://doi.org/10.2138/am-1998-3-405

Plank, T. (2014) 4.17 - The Chemical Composition of Subducting Sediments. In Holland, H.D., Turekian, K.K. (Eds.) *Treatise on Geochemistry*. Second Edition, Elsevier, Oxford, 607–629. https://doi.org/10.1016/B978-0-08-095975-7.00319-3

Plank, T., Langmuir, C.H. (1988) An evaluation of the global variations in the major element chemistry of arc basalts. *Earth and Planetary Science Letters* 90, 349–370. https://doi.org/10.1016/0012-821X(88)90135-5

Plank, T., Kelley, K.A., Zimmer, M.M., Hauri, E.H., Wallace, P.J. (2013) Why do mafic arc magmas contain ~4 wt% water on average? *Earth and Planetary Science Letters* 364, 168–179. https://doi.org/10.1016/j.epsl.2012.11.044

Pogge von Strandmann, P.A.E., Burton, K.W., James, R.H., van Calsteren, P., Gislason, S.R., Sigfússon, B. (2008) The influence of weathering processes on riverine magnesium isotopes in a basaltic terrain. *Earth and Planetary Science Letters* 276, 187–197. https://doi.org/10.1016/j.epsl.2008.09.020

Pogge von Strandmann, P.A.E., Elliott, T., Marschall, H.R., Coath, C., Lai, Y.-J., Jeffcoate, A.B., Ionov, D.A. (2011) Variations of Li and Mg isotope ratios in bulk chondrites and mantle xenoliths. *Geochimica et Cosmochimica Acta* 75, 5247–5268. https://doi.org/10.1016/j.gca.2011.06.026

Putirka, K.D. (2005) Mantle potential temperatures at Hawaii, Iceland, and the mid-ocean ridge system, as inferred from olivine phenocrysts: Evidence for thermally driven mantle plumes. *Geochemistry, Geophysics, Geosystems* 6, Q05L08. https://doi.org/10.1029/2005GC000915

Putirka, K.D., Perfit, M., Ryerson, F.J., Jackson, M.G. (2007) Ambient and excess mantle temperatures, olivine thermometry, and active vs. passive upwelling. *Chemical Geology* 241, 177–206. https://doi.org/10.1016/j.chemgeo.2007.01.014

Regelous, M., Niu, Y., Abouchami, W., Castillo, P.R. (2009) Shallow origin for South Atlantic Dupal Anomaly from lower continental crust: Geochemical evidence from the Mid-Atlantic Ridge at 26°S. *Lithos* 112, 57–72. https://doi.org/10.1016/j.lithos.2008.10.012

Richter, F.M., Watson, E.B., Mendybaev, R.A., Teng, F.-Z., Janney, P.E. (2008) Magnesium isotope fractionation in silicate melts by chemical and thermal diffusion. *Geochimica et Cosmochimica Acta* 72, 206–220. https://doi.org/10.1016/j.gca.2007.10.016

Richter, F.M., Watson, E.B., Mendybaev, R., Dauphas, N., Georg, B., Watkins, J., Valley, J. (2009) Isotopic fractionation of the major elements of molten basalt by chemical and thermal diffusion. *Geochimica et Cosmochimica Acta* 73, 4250–4263. https://doi.org/10.1016/j.gca.2009.04.011

Robertson, R.E. (2002) *Volcanic geology of the pre-Soufriere rocks on St. Vincent, West Indies*. PhD Thesis, The University of the West Indies. https://uwispace.sta.uwi.edu/dspace/handle/2139/3509

Robinson, C.J. (1998) *Mantle melting and crustal generation at the very slow spreading Southwest Indian Ridge*. PhD Thesis, University of Cambridge. https://ethos.bl.uk/OrderDetails.do?uin=uk.bl.ethos.246520

Roeder, P.L., Emslie, R.F. (1970) Olivine-liquid equilibrium. *Contributions to Mineralogy and Petrology* 29, 275–289. https://doi.org/10.1007/BF00371276

Scambelluri, M., Pettke, T., Cannao, E. (2015) Fluid-related inclusions in Alpine high-pressure peridotite reveal trace element recycling during subduction-zone dehydration of serpentinized mantle (Cima di Gagnone, Swiss Alps). *Earth and Planetary Science Letter*s 429, 45–59. https://doi.org/10.1016/j.epsl.2015.07.060

Shimizu, N., Arculus, R.J. (1975) Rare earth element concentrations in a suite of basanitoids and alkali olivine basalts from Grenada, Lesser Antilles. *Contributions to Mineralogy and Petrology* 50, 231–240. https://doi.org/10.1007/BF00394850

Sigurdsson, H., Shepherd, J.B. (1974) Amphibole-bearing basalts from the submarine volcano Kick 'em-Jenny in the Lesser Antilles Island arc. *Bulletin of Volcanology* 38, 891. https://doi.org/10.1007/BF02597097

Stamper, C.C., Blundy, J.D., Arculus, R.J., Melekhova, E. (2014a) Petrology of Plutonic Xenoliths and Volcanic Rocks from Grenada, Lesser Antilles. *Journal of Petrology* 55, 1353–1387. https://doi.org/10.1093/petrology/egu027

Stamper, C.C., Melekhova, E., Blundy, J.D., Arculus, R.J., Humphreys, M.C.S., Brooker, R.A. (2014b) Oxidised phase relations of a primitive basalt from Grenada, Lesser Antilles. *Contributions to Mineralogy and Petrology* 167, 954. https://doi.org/10.1007/s00410-013-0954-6

Stewart, W.H. (1980) *Pacific explorer's map of Guam, America's tropical paradise: an adventure guide to sightseeing, shopping, beachcombing, water sports, and historical remnants of World War II, ancient Chamorro & Spanish artifacts*. Scale ca. 1:100,000. Economic Service Counsel. Map G9416.E635 1980.S8.

Stracke, A., Tipper, E.T., Klemme, S., Bizimis, M. (2018) Mg isotope systematics during magmatic progresses: Inter-mineral fractionation in mafic to ultramafic Hawaiian xenoliths. *Geochimica et Cosmochimica Acta* 226, 192–205. https://doi.org/10.1016/j.gca.2018.02.002

Sun, S.-s., McDonough, W.F. (1989) Chemical and isotopic systematics of oceanic basalts: implications for mantle composition and processes. In Saunders, A.D., Norry, M.J. (Eds.) *Magmatism in the Ocean Basins*, Geological Society, London, Special Publication 42, 313–345. https://doi.org/10.1144/GSL.SP.1989.042.01.19

Tang, M., Rudnick, R.L., Chauvel, C. (2014) Sedimentary input to the source of Lesser Antilles lavas: A Li perspective. *Geochimica et Cosmochimica Acta* 144, 43–58. https://doi.org/10.1016/j.gca.2014.09.003

Teng, F.-Z. (2017) Magnesium Isotope Geochemistry. *Reviews in Mineralogy and Geochemistry* 82, 219–287. https://doi.org/10.2138/rmg.2017.82.7

Teng, F.-Z., Li, W.-Y., Ke, S., Marty, B., Dauphas, N., Huang, S., Wu, F.-Y., Pourmand, A. (2010a) Magnesium isotopic composition of the Earth and chondrites. *Geochimica et Cosmochimica Acta* 74, 4150–4166. https://doi.org/10.1016/j.gca.2010.04.019

Teng, F.-Z., Li, W.-Y., Rudnick, R.L., Gardner, L.R. (2010b) Contrasting lithium and magnesium isotope fractionation during continental weathering. *Earth and Planetary Science Letters* 300, 63–71. https://doi.org/10.1016/j.epsl.2010.09.036

Teng, F.-Z., Dauphas, N., Helz, R.T., Gao, S., Huang, S. (2011) Diffusion-driven magnesium and iron isotope fractionation in Hawaiian olivine. *Earth and Planetary Science Letters* 308, 317–324. https://doi.org/10.1016/j.epsl.2011.06.003

Teng, F.-Z., Hu, Y., Chauvel, C. (2016) Magnesium isotope geochemistry in arc volcanism. *Proceedings of the National Academy of Sciences* 113, 7082–7087. https://doi.org/10.1073/pnas.1518456113

Tenner, T.J., Hirschmann, M.M., Withers, A.C., Hervig, R.L. (2009) Hydrogen partitioning between nominally anhydrous upper mantle minerals and melt between 3 and 5 GPa and applications to hydrous peridotite partial melting. *Chemical Geology* 262, 42–56. https://doi.org/10.1016/j.chemgeo.2008.12.006

Thirlwall, M.F., Graham, A.M. (1984) Evolution of high-Ca, high-Sr C-series basalts from Grenada, Lesser Antilles: the effects of intra-crustal contamination. *Journal of the Geological Society* 141, 427–445. https://doi.org/10.1144/gsjgs.141.3.0427

Thirlwall, M.F., Graham, A.M., Arculus, R.J., Harmon, R.S., Macpherson, C.G. (1996) Resolution of the effects of crustal assimilation, sediment subduction, and fluid transport in island arc magmas: Pb–Sr–Nd–O isotope geochemistry of Grenada, Lesser Antilles. *Geochimica et Cosmochimica Acta* 60, 4785–4810. https://doi.org/10.1016/S0016-7037(96)00272-4

Tipper, E.T., Galy, A., Gaillardet, J., Bickle, M.J., Elderfield, H., Carder, E.A. (2006). The magnesium isotope budget of the modern ocean: Constraints from riverine magnesium isotope ratios. *Earth and Planetary Science Letters* 250, 241–253. https://doi.org/10.1016/j.epsl.2006.07.037

Tollan, P.M.E., Bindeman, I., Blundy, J.D. (2012) Cumulate xenoliths from St. Vincent, Lesser Antilles Island Arc: a window into upper crustal differentiation of mantle-derived basalts. *Contributions to Mineralogy and Petrology* 163, 189–208. https://doi.org/10.1007/s00410-011-0665-9

Turner, S., Regelous, M., Hawkesworth, C., Rostami, K. (2006) Partial melting processes above subduction plates: Constraints from ^{231}Pa–^{235}U disequilibria. *Geochimica et Cosmochimica Acta* 70, 480–503. https://doi.org/10.1016/j.gca.2005.09.004

Ulmer, P. (1989) The dependence of the Fe^{2+}-Mg cation-partitioning between olivine and basaltic liquid on pressure, temperature and composition. *Contributions to Mineralogy and Petrology* 101, 261–273. https://doi.org/10.1007/BF00375311

van Soest, M.C. (2000) *Sediment subduction and crustal contamination in the Lesser Antilles island arc; the geochemical and isotopic imprints on recent lavas and geothermal fluids*. PhD Thesis, Vrije Universiteit, Amsterdam.

van Soest, M.C., Hilton, D.R., Macpherson, C.G., Mattey, D.P. (2002) Resolving Sediment Subduction and Crustal Contamination in the Lesser Antilles Island Arc: a Combined He–O–Sr Isotope Approach. *Journal of Petrology* 43, 143–170. https://doi.org/10.1093/petrology/43.1.143

Wang, S.-J., Teng, F.-Z., Li, S.-G., Zhang, L.-F., Du, J.-X., He, Y.-S., Niu, Y. (2017) Tracing subduction zone fluid-rock interactions using trace element and Mg-Sr-Nd isotopes. *Lithos* 290–291, 94–103. https://doi.org/10.1016/j.lithos.2017.08.004

Wang, Y., He, Y., Ke, S. (2020) Mg isotope frcationation during partial melting of garnet-bearing sources: An adakite perspective. *Chemical Geology*. 537, 119478. https://doi.org/10.1016/j.chemgeo.2020.119478

Westbrook, G.K., Mascle, A., Biju-Duval, B. (1984) Geophysics and the structure of the Lesser Antilles forearc. In Biju-Duval, B., Moore, J.C., Bergen, J.A., Blackinton, G., Claypool, G.E., *et al.* (Eds.) *Initial Reports of the Deep Sea Drilling Program*, 78A, U.S. Govt. Printing Office, Washington, 23–28. https://doi.org/10.2973/dsdp.proc.78a.102.1984

White, W.M., Dupré, B. (1986) Sediment subduction and magma genesis in the Lesser Antilles: Isotopic and trace element constraints. *Journal of Geophysical Research: Solid Earth* 91, 5927–5941. https://doi.org/10.1029/JB091iB06p05927

Woodhead, J.D. (1988) The Origin of Geochemical Variations in Mariana Lavas: A General Model for Petrogenesis in Intra-Oceanic Island Arcs? *Journal of Petrology* 29, 805–830. https://doi.org/10.1093/petrology/29.4.805

Xiao, Y., Teng, F.-Z., Zhang, H.-F., Yang, W. (2013) Large magnesium isotope fractionation in peridotite xenoliths from eastern North China craton: Product of melt–rock interaction. *Geochimica et Cosmochimica Acta* 115, 241–261. https://doi.org/10.1016/j.gca.2013.04.011

Xiao, Y., Teng, F.-Z., Su, B.-X., Hu, Y., Zhou, M.-F., Zhu, B., Shi, R.-D., Huang, Q.-S., Gong, X.-H., He, Y.-S. (2016) Iron and magnesium isotopic constraints on the origin of chemical heterogeneity in podiform chromitite from the Luobusa ophiolite, Tibet. *Geochemistry, Geophysics, Geosystems* 17, 940–953. https://doi.org/10.1002/2015GC006223

Xu, Y., Zhu, D., Li, X., Liu, J. (2020) Why magnesium isotope fractionation is absent from basaltic melts under thermal gradients in natural settings. *Geological Magazine* 157, 1144–1148. https://doi.org/10.1017/S0016756819001304

Yang, W., Teng, F.-Z., Zhang, H.-F. (2009) Chondritic magnesium isotopic composition of the terrestrial mantle: A case study of peridotite xenoliths from the North China craton. *Earth and Planetary Science Letters* 288, 475–482. https://doi.org/10.1016/j.epsl.2009.10.009

Zhang, H.L., Cottrell, E., Solheid, P.A., Kelley, K.A., Hirschmann, M.M. (2018) Determination of $Fe^{3+}/\Sigma Fe$ of XANES basaltic glass standards by Mössbauer spectroscopy and its application to the oxidation state of iron in MORB. *Chemical Geology* 479, 166–175. https://doi.org/10.1016/j.chemgeo.2018.01.006

Zhong, Y., Chen, L.-H., Wang, X.-J., Zhang, G.-L., Xie, L.-W., Zeng, G. (2017) Magnesium isotopic variation of oceanic island basalts generated by partial melting and crustal recycling. *Earth and Planetary Science Letters* 463, 127–135. https://doi.org/10.1016/j.epsl.2017.01.040